Supporting Information

A study of [2+2] cycloaddition–retroelectrocyclization in water: observation of substrate-driven transient-nanoreactor-induced new reactivity

K. M. Neethu,[†] Kritika Nag,[†] Arif Hassan Dar,[†] Ashima Bajaj,[†] S. Arya Gopal,[‡] Vijayendran Gowri,[†] Mithilesh Nagpure,[†] Shaifali Sartaliya,[†] Raina Sharma,[†] Arun Kumar Solanki,[†] Md. Ehesan Ali,[†] Azhagumuthu Muthukrishnan,[‡] Govindasamy Jayamurugan*[,†]

[a]Institute of Nano Science and Technology, Knowledge City, Sector 81, SAS Nagar, Manauli PO, Mohali, Punjab 140306, India

[b]School of Chemistry, Indian Institute of Science Education and Research Thiruvananthapuram, Thiruvananthapuram 695551, Kerala, India

Email: jayamurugan@inst.ac.in.

A Experimental section

A1 General methods and materials

All reagents and solvents were obtained from commercial suppliers (Sigma-Aldrich, Spectrochem, and TCI India) and used without further purification. Acetonitrile (CH_3CN, HPLC Grade,) and dichloromethane (CH_2Cl_2) was distilled over anhydrous CaH_2 under the nitrogen (N_2) atmosphere, protected by 4Å molecular sieves under the argon atmosphere before each experiment. Column chromatography (CC) was carried out with neutral silica gel. Thin-layer chromatography (TLC) was performed on precoated plastic sheets of silica gel G/UV-254 of 0.2 mm thickness (MachereyNagel, Germany) using appropriate solvents and visualized with UV light (λ = 254 nm). Melting points (M.p.) were measured in open capillaries with a Stuart (automatic melting point SMP50) apparatus and are uncorrected. ^{1}H NMR spectra were measured on Bruker Avance II 400 MHz instrument at 298 K in $CDCl_3$, acetone-d_6, and DMSO-d_6. Chemical shifts (δ) are reported in ppm downfield from $SiMe_4$, with the residual solvent signal. Coupling constants (J) are given in Hz. The apparent resonance multiplicity is described as s (singlet), d (doublet), t (triplet), and m (multiplet). Transmission spectra were measured using ATR FT-IR Bruker Vertex 70; signal designations; s (strong), m (medium), and w (weak). UV/vis spectra were measured in a quartz cuvette of 1 cm at 298 K on a Shimadzu UV/vis (UV 2600) spectrophotometer. The absorption maxima (λ_{max}) are reported in nm with the extinction coefficient (ε) in $dm^3\ mol^{-1}\ cm^{-1}$ in brackets. ESI-MS spectra were measured on a Bruker maXis ESI-Q-TOF spectrometer. The most important signals are reported in *m/z* units with M^+ as the molecular ion. Fluorescence spectra were measured on an Edinburgh FS5 spectrophotometer in a 1 cm quartz cuvette.FE-SEM analysis was performed on model JSM6100(Jeol) with image analyzer. The dried drop casted sample was mounted on stubs with the help of double-stick tape and sputtered with a film of gold. Confocal fluorescent microscopy was performed on a Ziess LSM880 confocal microscope (Carl Zeiss, Thornwood, New York). A suspension without further dilution of samples was drop casted on a glass slide, trapped by a glass cover slip. Dynamic light scattering was performed to determine the particle size distribution using Zetasizer Nano ZSP; Model-ZEN5600; MalvernInstruments LTD., Worcestershire, UK.

Electrochemistry: The redox properties were measured by cyclic voltammetry. Tetrabutylammonium perchlorate (Bu_4NClO_4, TBAP) (Sigma-Aldrich, electrochemical grade) was used as the supporting electrolyte without further purification. Solutions (1 mM) of the compounds in dry CH_2Cl_2 and CH_3CN for compounds **2a** and **3a**, respectively were used for

all studies. The electrochemical studies were conducted using PARSTAT potentiostat. Three electrode system in which, the working electrode was Glassy Carbon electrode (3 mm dia, CH Instruments, USA). The GC electrode was polished with 0.05 µm alumina slurry to mirror finish and sonicated. The Ag/Ag^+ (0.01 M) electrode is used as the quasi-reference electrode prepared from the same supporting electrolyte in acetonitrile. Later the potential was corrected with ferrocene/ferrocenium-ion using ferrocene as an internal standard. Platinum wire is used as the counter electrode. Voltammetry studies were conducted in nitrogen atmosphere.

A2 [2+2] CA-RE reaction of DMA and TCNE in water

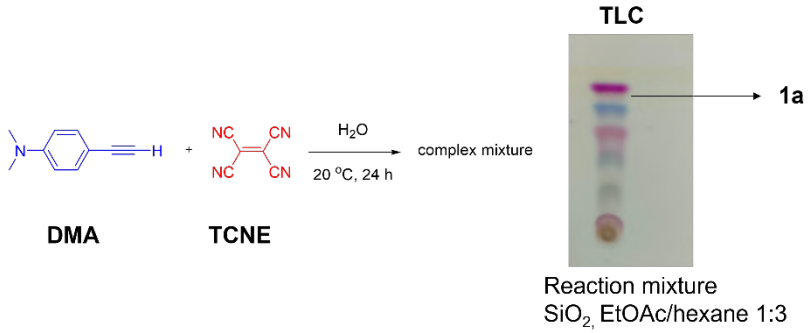

Scheme S1. Synthetic scheme for the water-mediated [2+2] CA-RE reaction of DMA and TCNE (inset: TLC image of the reaction mixture).

A3 Synthetic procedures and characterization of the products

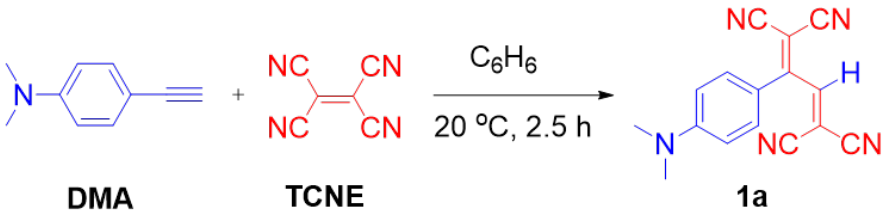

Scheme S2. Synthesis of **1a** (**DMA-TCBD)** from DMA and TCNE in organic solvent.[S1]

*Synthesis of **1a** (CA-RE reaction) in organic solvent*:[S1] To a solution of 4-ethynyl-*N*,*N*-dimethylaniline (DMA) (100 mg, 0.69 mmol) in anhydrous C_6H_6 (5 mL) added TCNE (88 mg, 0.69 mmol). The reaction mixture was stirred for 2.5 h at 20 °C. Upon reaction completion, the mixture was concentrated in *vacuo* and purified by column chromatography. Eluted with hexane/EtOAc 6:4 to afford **1a**[S1] (169 mg, 90%) as a purple solid. R_f = 0.3 (SiO_2; hexane/EtOAc 7:3); M.p. 144–145 °C; ^{1}H NMR ($CDCl_3$, 400 MHz, 298 K): δ = 3.16 (s, 6 H), 6.75 (d, J = 12 Hz, 2 H), 7.50 (d, J = 8 Hz, 2 H), 8.02 ppm (s, 1 H); ^{13}C NMR (100 MHz, $CDCl_3$): δ = 40.3, 78.0, 97.2, 109.1, 111.5, 112.1, 113.1, 113.7, 117.7, 132.1, 154.3, 156.7,

158.8 ppm; FT-IR (ATR) $\tilde{\nu}$ = 3037 (m), 2922 (m), 2213 (s), 1713 (s), 1598 (s), 1531 (s), 1479 (s), 1380(m), 1347 (s), 1293 (w), 1293 (m), 1117 (m), 1089 (m), 939 (w), 831 (w), 722 cm^{-1} (w); HRMS (ESI): *m/z* (%) calcd. for $C_{16}H_{11}N_5^+$, $[M]^+$ 273.1014; found: 273.1022.

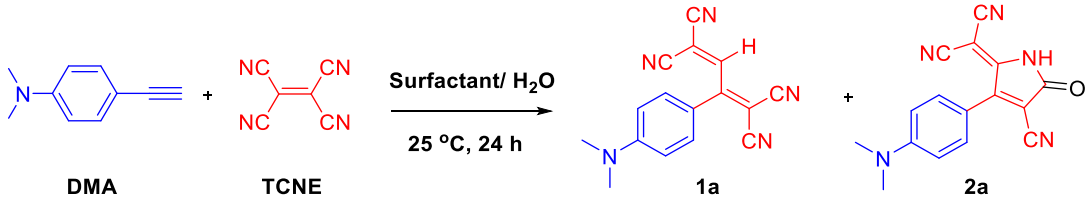

Scheme S3. Synthesis of **1a** and **2a** in water using surfactant from DMA and TCNE.

*Synthesis of **1a** and **2a** in water using surfactant:* TCNE (88 mg, 0.69 mmol) was added to a solution of 4-ethynyl-*N*,*N*-dimethylaniline (DMA) (100 mg, 0.69 mmol) in 10 mL of surfactant/H_2O solution. The reaction mixture was stirred for 24 h at 25 °C under N_2. 30 mL of EtOAc was added and the organic layer was separated. The aqueous layer was washed further with EtOAc (3 × 10 mL) and the combined organic layer was dried over anhydrous Na_2SO_4. The solution was filtered and dried. Purified by CC. Eluted with hexane/EtOAc 1:1 to afford **2a** (10 mg, 5%) as a dark purple shiny solid; R_f = 0.3 (SiO_2; hexane/EtOAc 6:4); M.p. 346 °C; ^{1}H NMR (400 MHz, $CDCl_3$, 298 K): δ = 3.16 (s, 6 H; H_a), 6.79 (d, *J* = 9.1 Hz, 2 H; H_b), 7.59 (d, *J* = 9.1 Hz, 2 H; H_c), 8.41 ppm (s, 1 H; H_d); ^{13}C NMR (100 MHz, $CDCl_3$, 298 K): δ = 40.4, 67.5, 96.2, 110.8, 111.9, 113.0, 132.4, 154.5, 156.0, 159.7, 162.9 ppm; FT-IR (ATR) $\tilde{\nu}$= 3234 (s), 2922 (m), 2227 (s), 1734 (s), 1605 (s), 1564 (s), 1523 (s), 1388 (s), 1340 (m), 1191 (m), 1103, 892 (w), 824 (w), 756 (w) cm^{-1}; HR-MS (ESI): *m/z* (%) calcd. for $C_{16}H_{12}N_5O^+$, $[M+H]^+$ 290.1036; found: 290.0791.

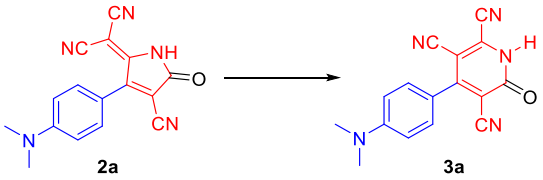

Scheme S4. Synthesis of **3a** from **2a**

*Synthesis of **3a** from **2a**:*

Solvent-mediated Procedure-1: Crystals of compound **2a** (20 mg, 0.07 mmol) was dissolved in EtOAc or CH_3CN (5 mL) and kept the solution on standby for 8 h at 25 °C. The colour change from blue to pink was observed indicating the formation of **3a** also the conversion was monitored by TLC. Evaporation of the solvent and drying afforded pink solid **3a** (19 mg, 98%); R_f = 0.2 (SiO_2; hexane/EtOAc 6:4).

Silica gel mediated Procedure-2: Silica gel (3 mg) was added to a solution of compound **2a** (20 mg, 0.07 mmol) in CH_2Cl_2 (5 mL) and the reaction mixture was stirred for 4 h at 25 ºC. After completion of the reaction the solution was filtered using filter paper and washed with CH_2Cl_2. The CH_2Cl_2 solution was evaporated and dried in vacuo to provide the pink solid **3a** (16 mg, 80%); R_f = 0.2 (SiO_2; hexane/EtOAc 6:4).

M.p. 365 °C; ^{1}H NMR (400 MHz, acetone-d_6, 298 K): δ = 3.20 (s, 6 H; H_a), 6.92 (d, J = 9.4 Hz, 2 H; H_b), 8.36 (d, J = 9.4 Hz, 2 H; H_c), 10.27 ppm (s, 1H; H_d); ^{13}C NMR (100 MHz, acetone-d_6): δ = 39.2, 96.7, 112.1, 113.9, 115.0, 132.7, 147.5, 154.1, 167.3, 169.8 ppm; FT-IR (ATR) $\tilde{\nu}$ = 3251 (s), 2921 (s), 2854 (m), 2219 (s), 1763 (s), 1718 (s), 1707 (s), 1600 (s), 1506 (s), 1356 (w), 1211 (m), 1089 (m), 971 (w), 939 (w), 832 (w), 754 cm^{-1} (w); HRMS (ESI): *m/z* (%) calcd. for $C_{16}H_{12}N_5O^+$, $[M+H]^+$ 290.1036; found, 290.1018.

A4. General procedure for optimization in surfactants

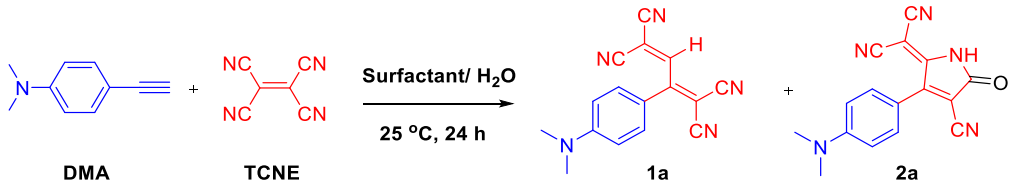

Scheme S5. General procedure for the CA-RE reaction in water-surfactant monitored by ^{1}H-NMR spectroscopy.

TCNE (8.8 mg, 0.069 mmol) and DMA 4,4'-(ethyne-1,2-diyl)bis(*N*,*N*'-dimethylaniline) (10 mg, 0.069 mmol) was suspended into a 2 mL of appropriate concentration (see Table 1 in the main manuscript) of aqueous solution of surfactant at 25 °C under N_2 atmosphere. After stirring (300 rpm) for 24 h, 10 mL of EtOAc was added and the organic layer was separated. The aqueous layer further washed with EtOAc (5 mL × 5) and the combined organic layer was dried over anhydrous Na_2SO_4. The solution was filtered and vacuum dried to obtain crude mixture. The crude reaction mixture was dissolved in deuterated DMSO (0.6 mL) which contains 0.2 mmol of bromonitromethane ($BrCH_2NO_2$) as internal standard for measuring ^{1}H NMR spectra. The yield was calculated according to the equation 1,

$$I_A/ I_B = H_A\ C_A/H_B\ C_B \qquad (1)$$

A = Sample, B = Standard, I = Signal Intensity (integral), C = Concentration, H = Number of protons.

B Spectra of newly synthesized compounds

B1 NMR (^{1}H and ^{13}C) spectra

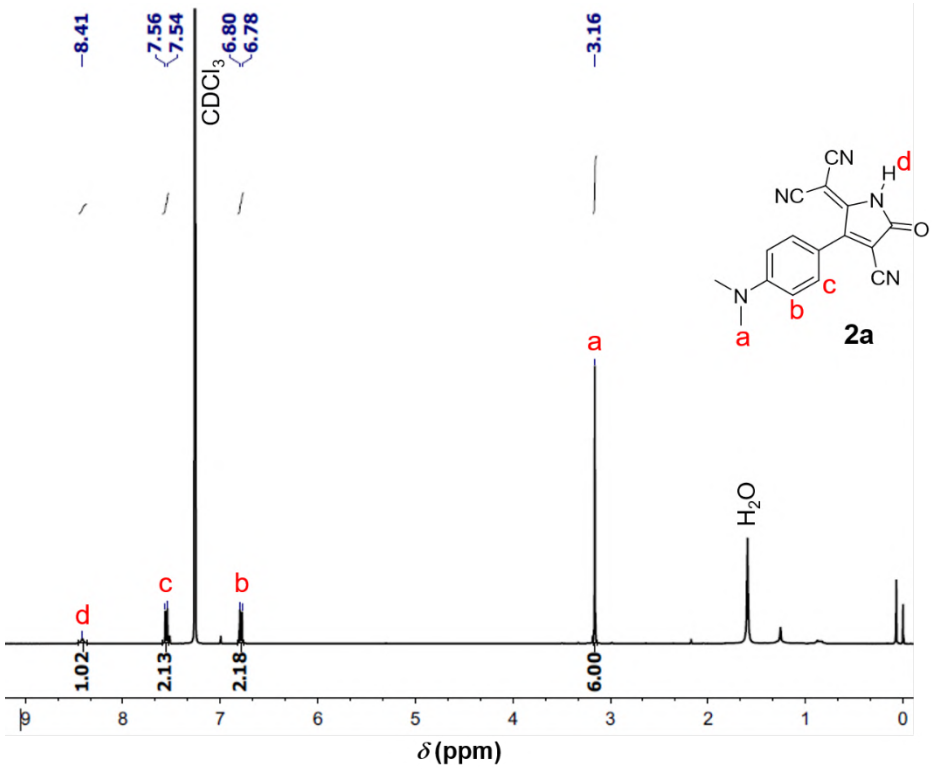

Fig. S1. 400 MHz ^{1}H NMR spectrum of **2a** recorded at 298 K in $CDCl_3$.

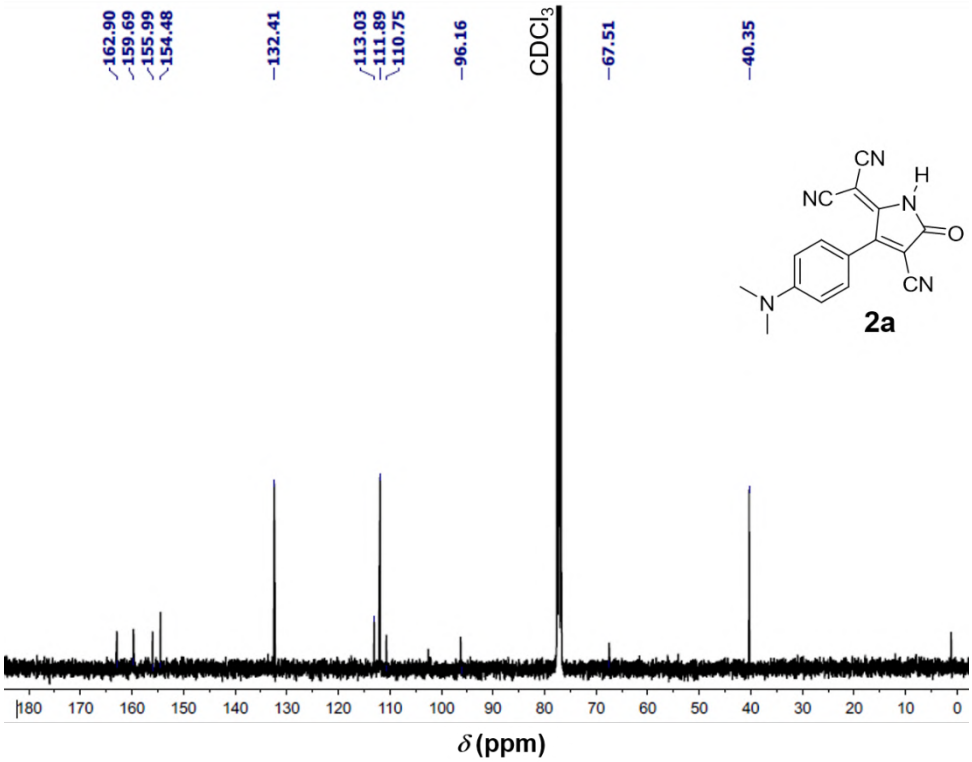

Fig. S2. 100 MHz ^{13}C NMR spectrum of **2a** recorded at 298 K in $CDCl_3$.

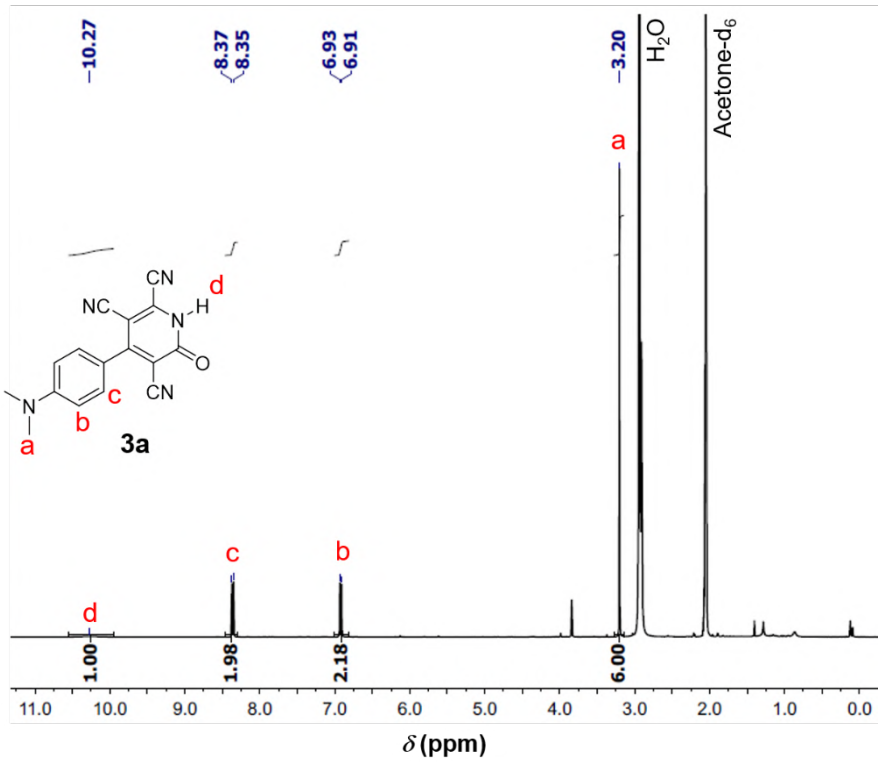

Fig. S3. 400 MHz ^{1}H NMR spectrum of **3a** recorded at 298 K in acetone-d$_6$.

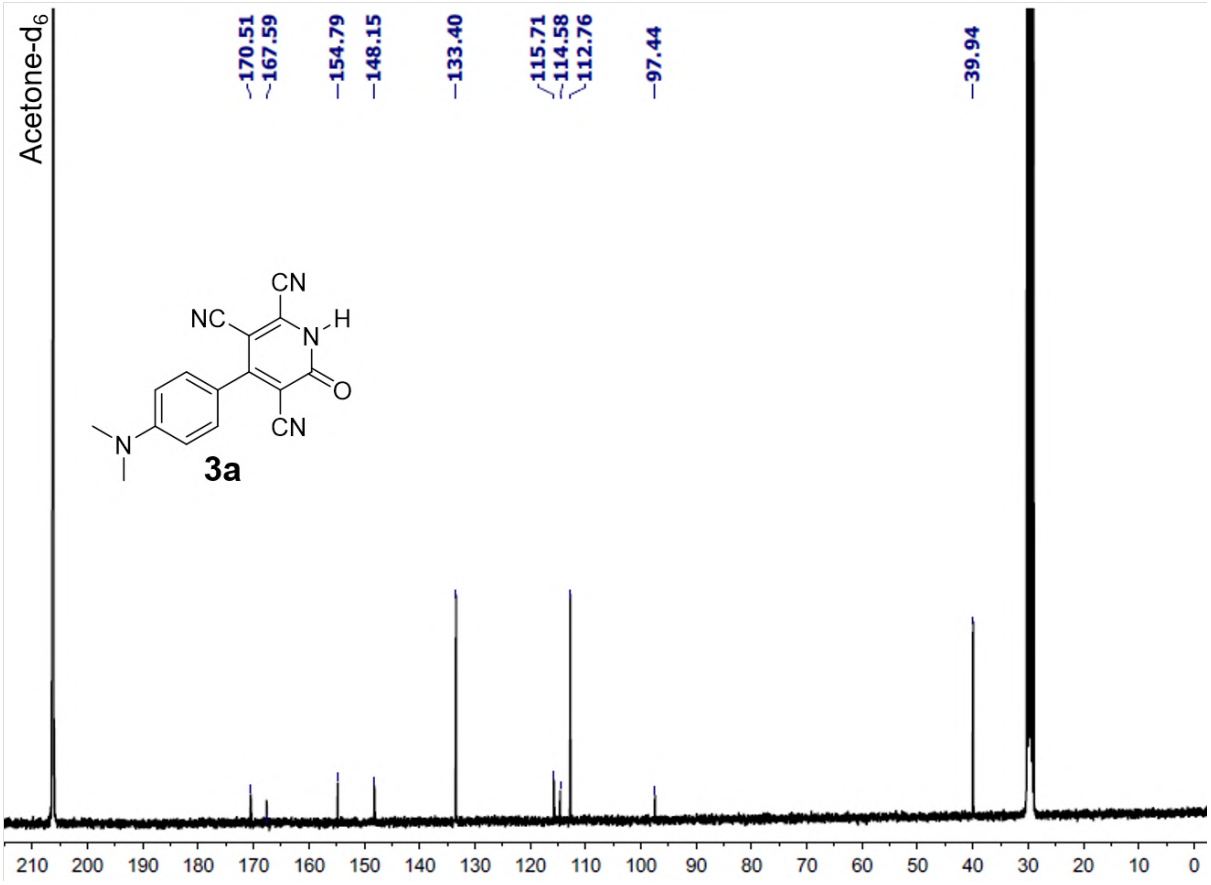

Fig. S4. 100 MHz ^{13}C NMR spectrum of **3a** recorded at 298 K in acetone-d$_6$.

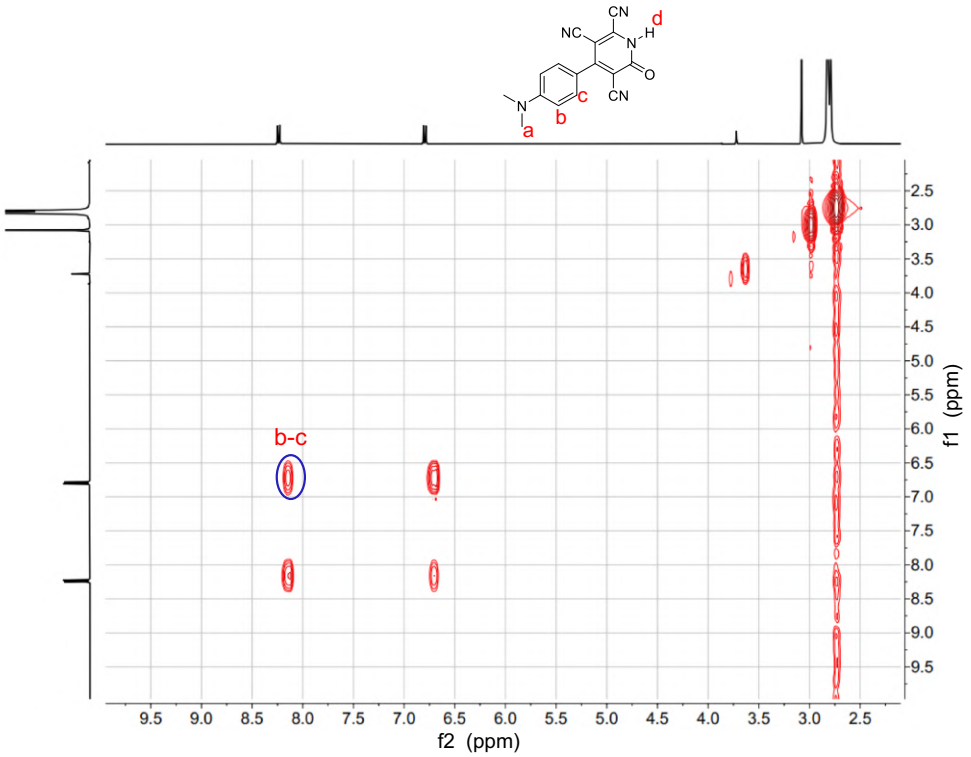

Fig. S5. COSY NMR spectrum of **3a** recorded at 298 K in acetone-d_6.

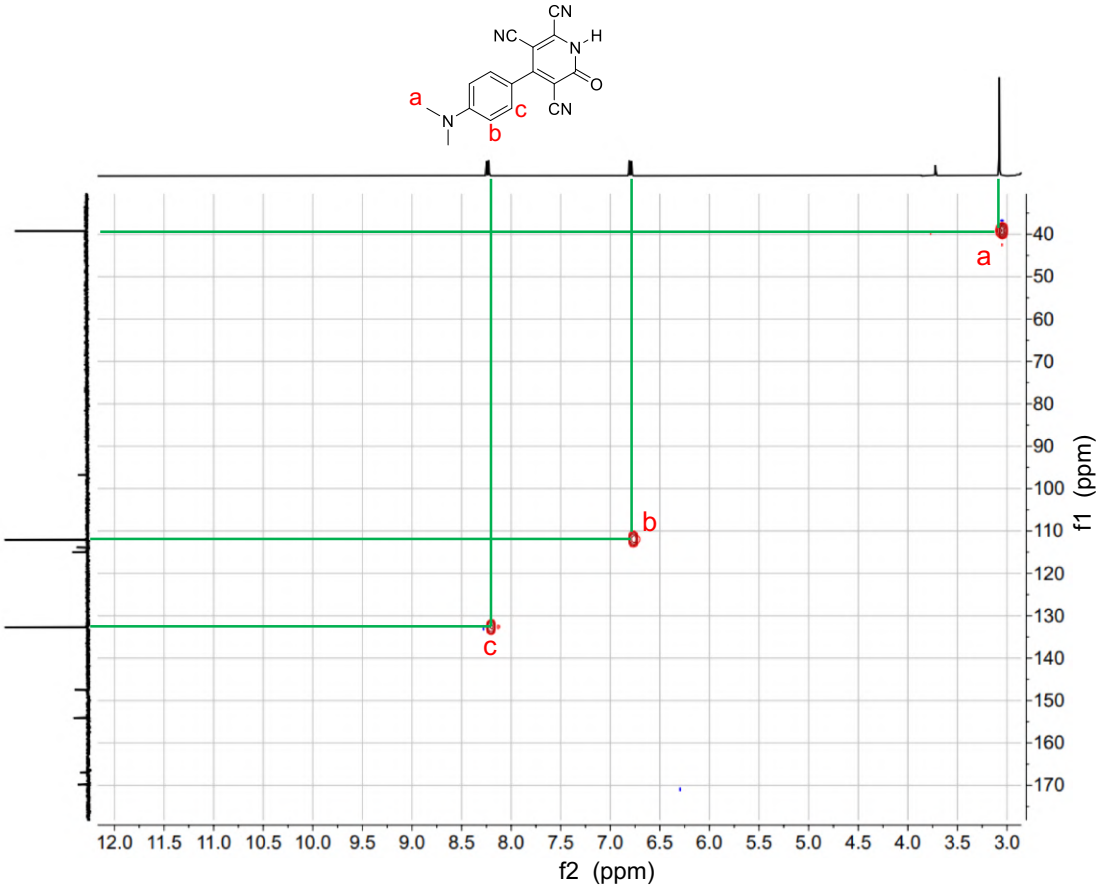

Fig. S6. HSQC NMR spectrum of **3a** recorded at 298 K in acetone-d_6.

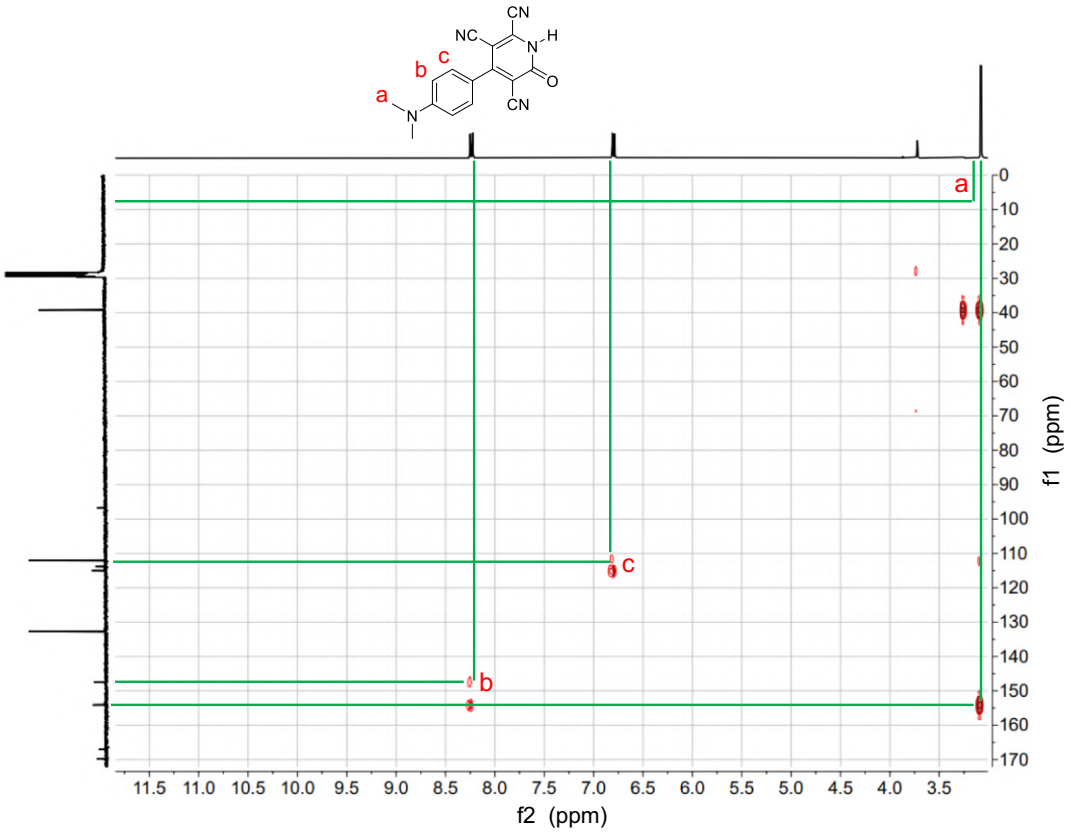

Fig. S7. HMBC NMR spectrum of **3a** recorded at 298 K in acetone-d_6.

B2 ESI-MS spectra of newly synthesized compounds

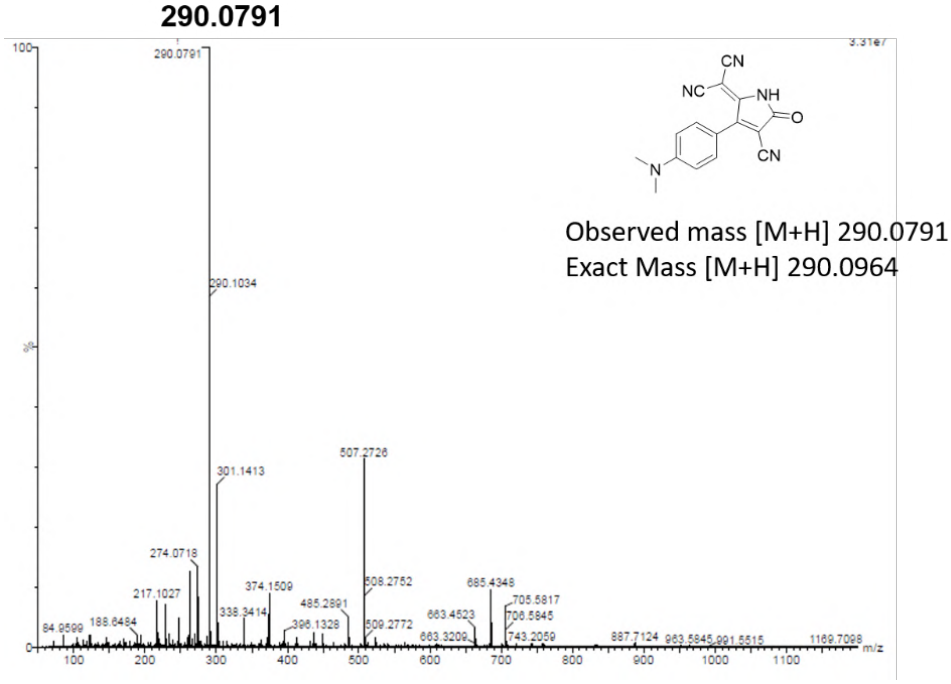

Fig. S8. High-resolution ESI-MS spectrum of **2a**

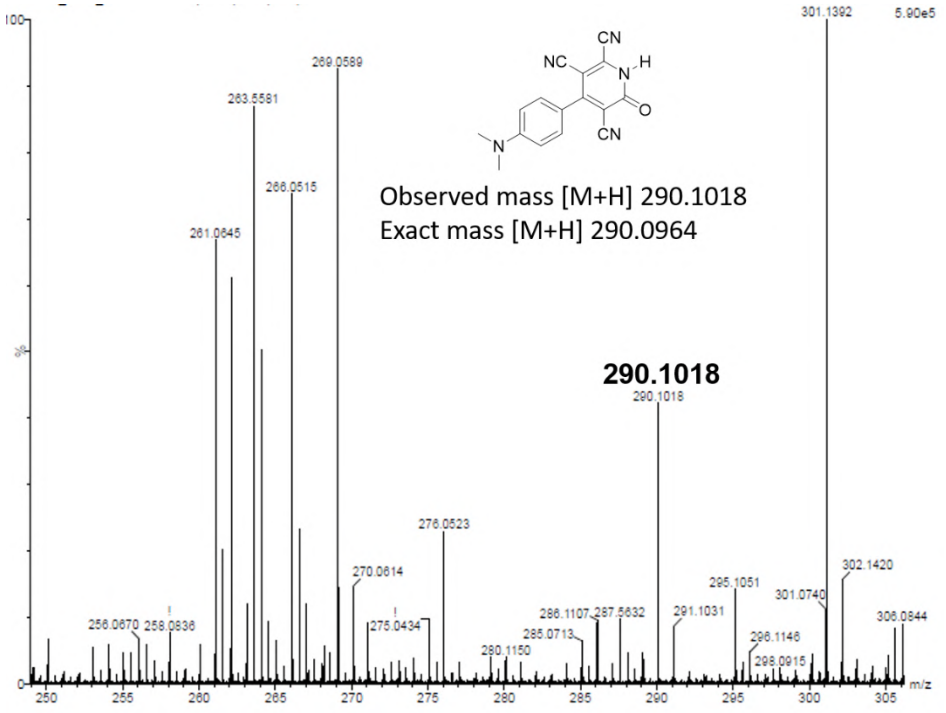

Fig. S9. High-resolution ESI-MS spectrum of **3a**

B3 FT-IR spectra

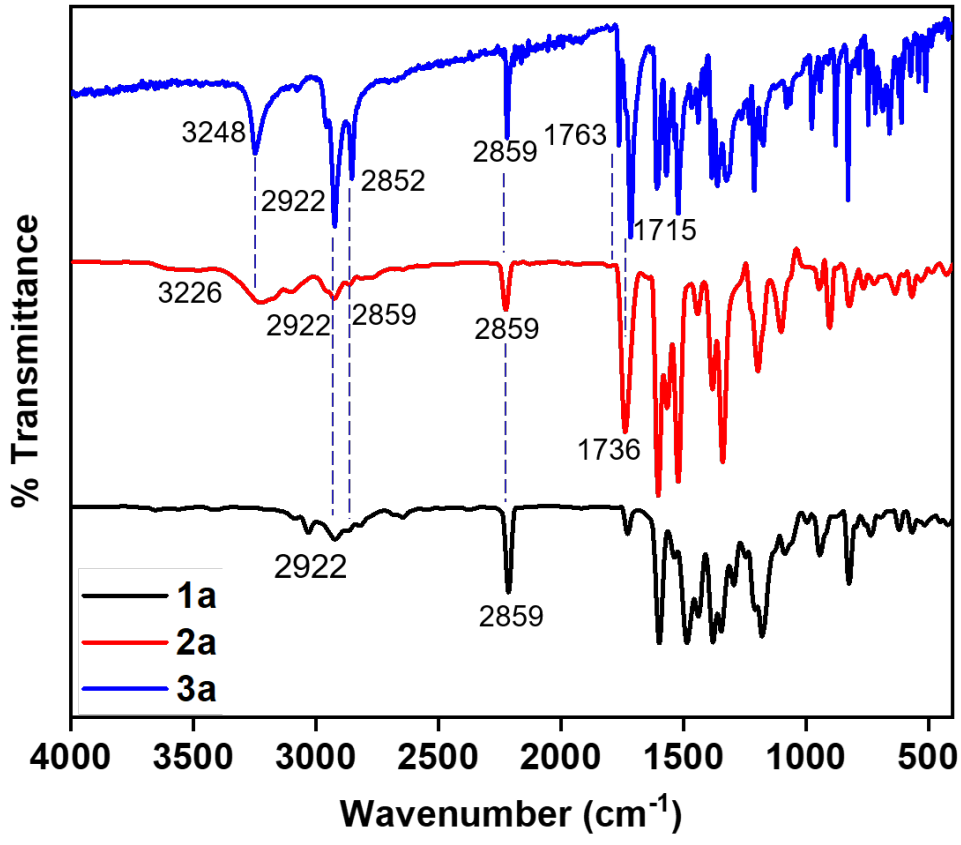

Fig. S10. FT-IR spectra of **1a, 2a** and **3a**.

C X-ray data of 2a

X-Ray crystal structure of **2a** (CCDC 2216738, 298 K). Detailed crystallographic data and structural refinement parameters are summarized as follows. A dark purple shiny (cubic dimensions ca. 0.24 × 0.31 × 0.28 mm) was obtained from CH_2Cl_2/hexane solution at 20 °C. Crystal data for $C_{16}H_{11}N_5O$, Mr = 289.1, Monoclinic, space group P $2_1/c$ (14), *D*calcd = 1.308 g cm^{-3}, Z = 5, a = 19.6578(10) Å, b = 7.7477(3) Å, c = 20.2282(9) Å, V = 2915.86 $Å^3$; m = 0.088 mm^{-1}. Numbers of measured and unique reflections were 8599 and 2746, respectively (Rint = 0.0248, Rsigma = 0.0296). Final R(F) = 0.0600, wR(F2) = 0.1928.

Single-crystal X-ray diffraction data were collected using a Super-Nova (Mo) X-ray diffractometer equipped with a microfocus sealed X-ray tube Mo-Kα (λ = 0.71073 Å) X-ray source, and HyPix3000 detector with increasing ω (width of 0.3 per frame) at a scan speed of either 5 or 10 s/frame. The data were deduced using CrysAlisPro software and the space group determination was done using Olex2.[S2] The structure was solved with the SIR2004[S3] structure solution program using Direct Methods and refined with the ShelXL[S4] refinement package using Least Squares minimization through Olex2 suite. The crystallographic information file is deposited with the CCDC number 2216738. This data can be obtained free of charge from The Cambridge Crystallographic Data Centre, 12 Union Road, Cambridge CB2 1EZ, UK (fax: +44(1223)-336-033; e-mail: deposit@ccdc.cam.ac.uk), or via www.ccdc.cam.ac.uk/data_request/cif

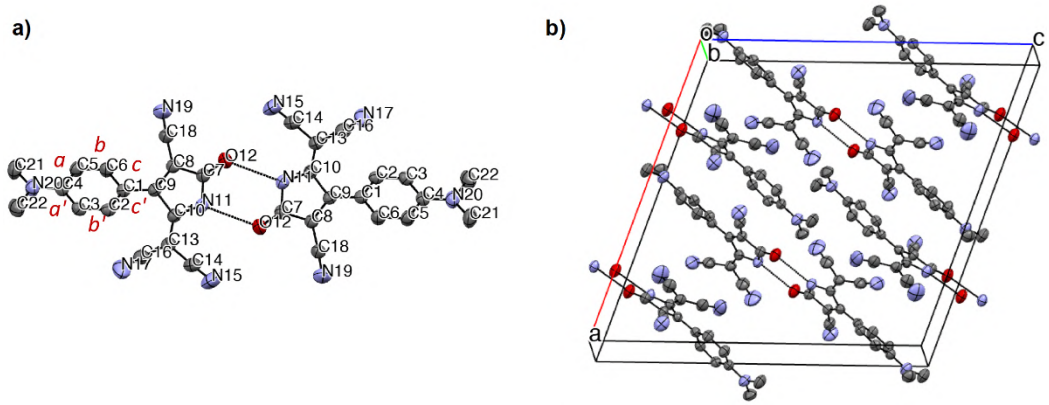

Fig. S11. a) ORTEP plot of two molecules of **2a** connected through hydrogen bonding (arbitrary numbering). Atomic displacement parameters are drawn at 50% probability level. Selected bond lengths [Å], angles [°], and torsional angles [°]: C1–C2: 1.400(2), C1–C9: 1.437, C1–C6: 1.402, C2–C3: 1.365(2), C2–H2: 0.930, C3–C4: 1.404(2), C3–H3: 0.930, C4–C5: 1.404(2), C4–N20: 1.357, C5–C6: 1.367(2), C5–H5: 0.930, C6–H6: 0.930, C7–C8: 1.460(2), C7–O12: 1.215(2), C7–N11: 1.380(2), N11–H11: 0.860, C8–C18: 1.416(2), C8–C9:

1.1.370(2), C9–C10: 1.1.481(2), C10–C13: 1.358(2), C10-N11: 1.369, C13–C14: 1.432(2), C13–C16: 1.429, C14–N15: 1.134(2), C16–N17: 1.134, C18–N19: 1.139(2), C21-N20: 1.455, C22-N20: 1.449. The quinoid character (δ_r) was calculated [Eq. (2)][S5] to understand the extent of intramolecular charge transfer (ICT) present in the molecule by comparing the bond length alternations of the donor substituted benzene ring in the structure and from unsubstituted benzene ring for which the δ_r value is zero. The method has been successfully used to characterize for the previously reported TCBDs.[S6]

$$\delta r = \{[(a + a') - (b + b')]/2 + [(c + c') - (b + b')]/2\}/2 \qquad (2)$$

The value of δr was calculated to be 0.036 which is comparable with the DMA substituted TCBDs[S7] showing the efficient ICT property.

b) Arrangement of neighboring molecules in the crystal packing of **2a** (Hydrogen atoms are omitted for clarity).

D. Mechanistic Studies

D1. Control study for the enol-intermediate I over amide tautomer

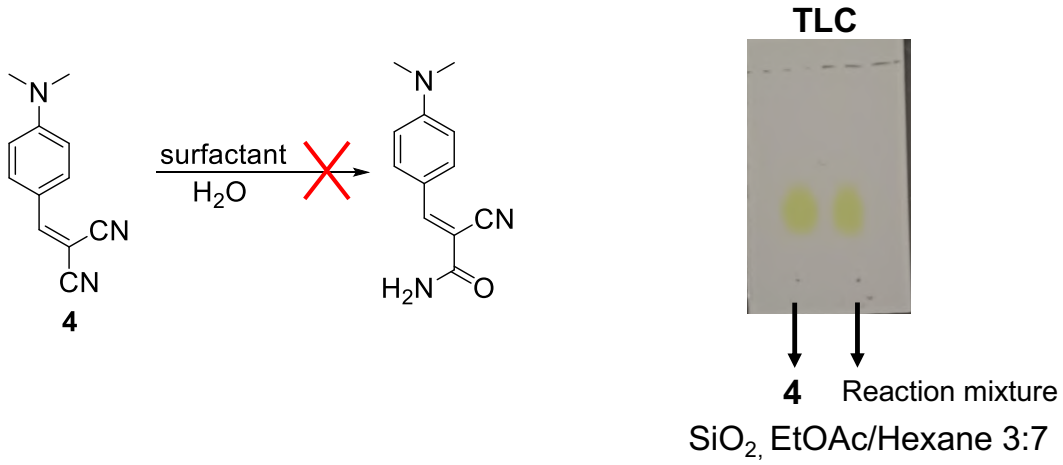

Scheme S6. Testing of water addition to generate amide functionality in reaction of **4** under surfactant conditions.

D2. Deuterium exchange study

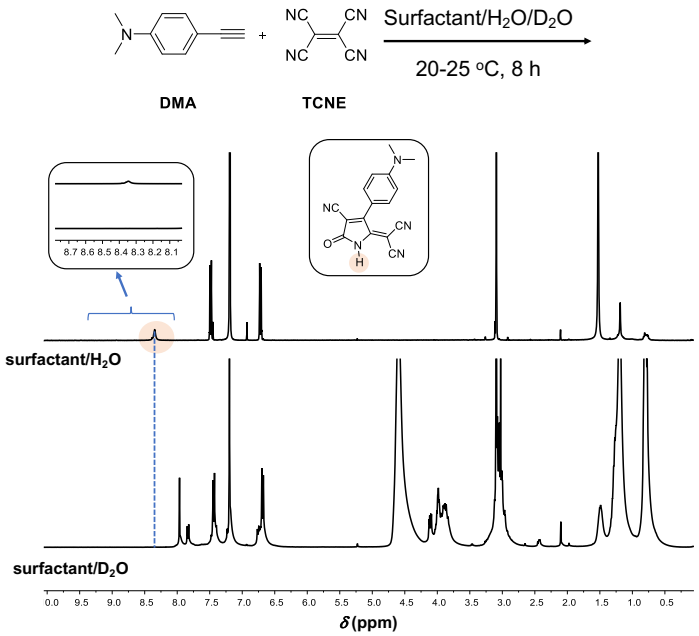

Fig. S12. ^{1}H-NMR spectra of reaction conducted in a) H_2O (purified **2a**) and in b) D_2O (reaction mixture).

D3. Shape transition study

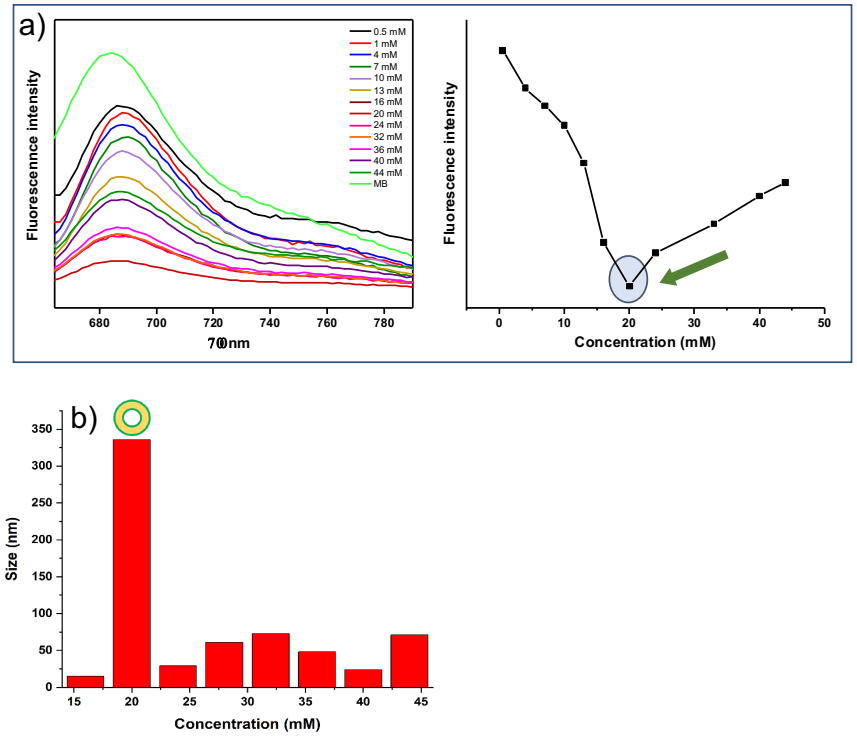

Fig. S13. a) Determination of shape transition using methylene blue (MB) fluorescent probe (λ_{ex}=650 nm) performed at various concentration of Tween 20 with DMA, b) Corresponding size measurements of transient structures using DLS.

D4. Control studies in mixture of organic solvents and water & water as an additive.

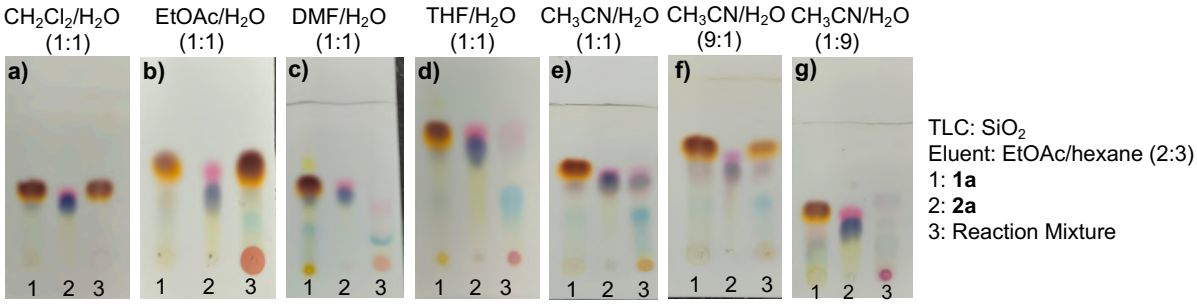

Fig. S14. TLC of the reaction performed in the organic solvents and water at different ratios. Note: In the presence of EtOAc and SiO_2, **2a** tends to convert to **3a**, resulting in the appearance of spot-2 in TLC as a mixture of **2a** and **3a** (blue and pink colors), although in the reaction mixture 3a is not present.

E Photophysical (UV/Vis, electrochemical, DFT) and substrate scope studies

E1. UV/Vis Studies

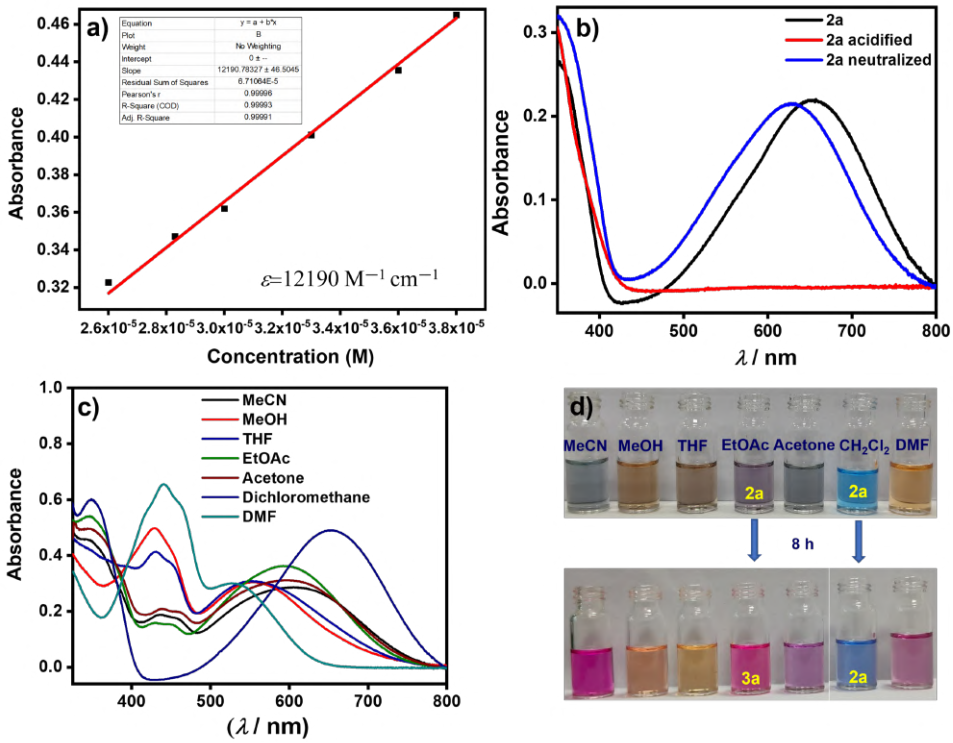

Fig. S15. UV/Vis studies of **2a** (10^{-5} M) a) molar extinction coefficient, b) acid-base titration in CH_2Cl_2 (10^{-5} M) when acidified with TFA and neutralized with Et_3N c) solvatochromism study (10^{-5} M), (d) naked eye visualization of color changes in different solvents.

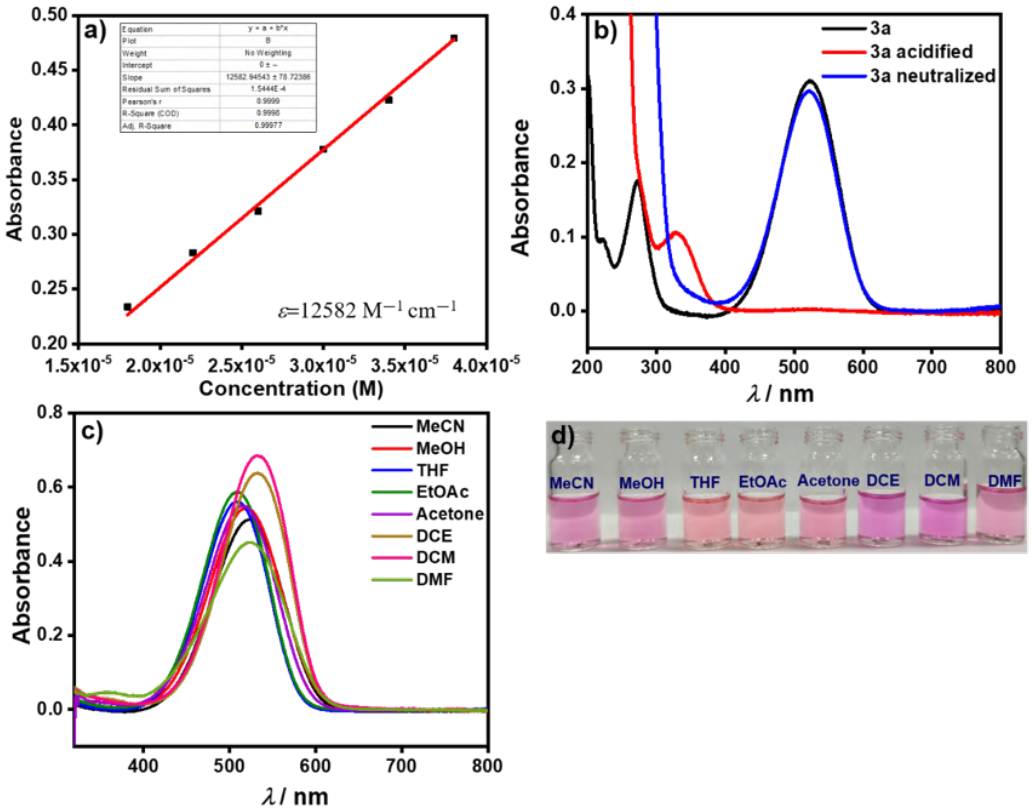

Fig. S16. UV/Vis studies of **3a** (10^{-5} M) a) molar extinction coefficient, b) acid-base titration in CH_3CN (10^{-5} M) when acidified with TFA and neutralized with Et_3N (c) solvatochromism study (10^{-5} M), (d) naked eye visualization of **3a** in different solvents.

E2. Electrochemistry Data

Cyclic voltammetry (CV) was performed to quantify the HOMO-LUMO gaps and redox behavior of compounds **2a** and **3a** in CH_2Cl_2 and CH_3CN, respectively in the presence of 0.1M Bu_4NClO_4 (Scan rate (v) = 0.1 V s^{-1}). The results are summarized in Table S1. In the case of **2a**, there is a peak around 1.37 V, which corresponds to irreversible oxidation and the first reversible reduction peak is observed at –0.81 V. The reduction peak shown near 1.1 V may be attributed to the species formed due to the irreversible oxidation of **2a**. The difference between the onset potentials of the first reduction and oxidation peaks is estimated as 2.04 eV for **2a**, in good agreement with the optical bandgap, estimated earlier for **2a**. Compound **3a** showed reversible redox behavior. Two reduction potentials were observed at –0.98 and –1.68 eV which might correspond to two distinct double bonds one attached with two nitrile groups and the other with DMA and nitrile substitution, respectively. This is further verified by DFT calculation using the B3LYP level of theory. Both ab initio calculations- (TD-DFT) and electrochemical- H-L gap matches well with the optical band gap (Section E2 & E3).

Table S1. Electrochemical data of **2a** and **3a** observed by cyclic voltammetry (CV) (Scan rate (v) = 0.1 V s^{-1}) in CH_2Cl_2 and CH_3CN, respectively (in the presence of 0.1M Bu_4NClO_4).

Compound	Peak parameters			
	$E°$ [V][a]	ΔE_p [mV][b]	E_p [V][c]	HOMO–LOMO (H–L) Gap [eV][d]
2a	0.025		1.37	2.04
3a	–0.81			
	–0.98			1.99
	–1.63			
	+0.83	–0.1		

[a]$E^o = (E_{pc} + E_{pa})/2$, where E_{pc} and E_{pa} correspond to the cathodic and anodic peak potentials, respectively. [b]$\Delta E_p = E_{pa} - E_{pc}$. [c]$E_p$ = Irreversible peak potential. [d]H–L = $E_{red,1} + E_{ox,1}$. The difference between onset potentials of first reduction and oxidation peaks defines the HOMO-LUMO gap.

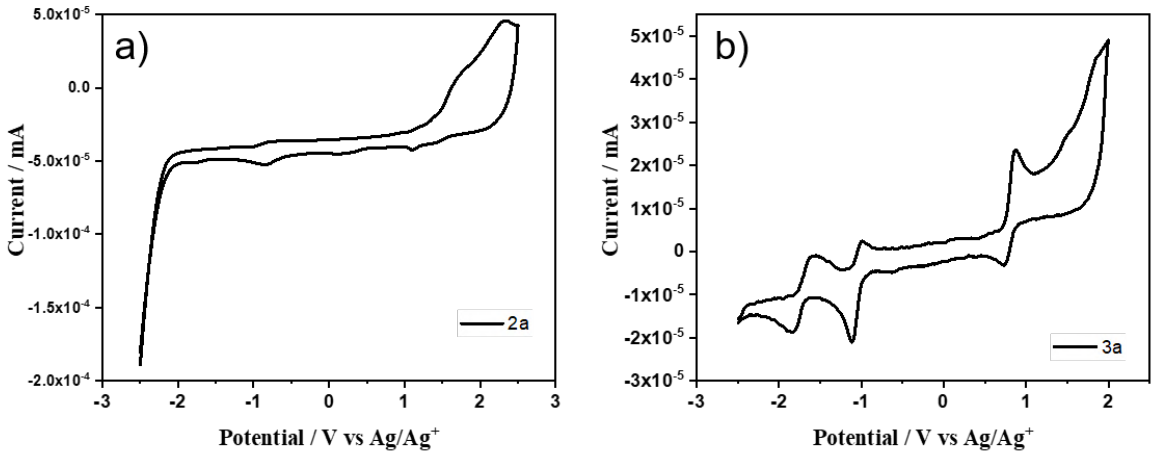

Fig. S17. Cyclic voltammograms of a) **2a** in CH_2Cl_2, b) **3a** in CH_3CN on GC electrode containing 0.1M Bu_4NClO_4 as a supporting electrolyte. Scan rate is 0.1 V s^{-1}.

E3 Ab Initio Calculations

All the electronic structure calculations were performed with ORCA program. Geometry optimizations were performed at DFT level using B3LYP/TZVP method.[S8] For all the atoms, we employed def2-TZVP basis set. The calculations were accelerated by employing the resolution of identity (RI) approximation with the large grid 5. To compute the exchange terms effectively 'Chain of Spheres Exchange' (COSX) is used.

Molecular Orbitals

Table S2. The frontier molecular orbitals involved of 1-4 calculated at DFT B3LYP/def2-TZVP level with isovalue = 0.01.

	2a	**3a**
LUMO+2	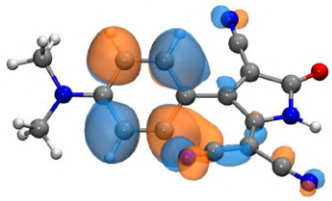	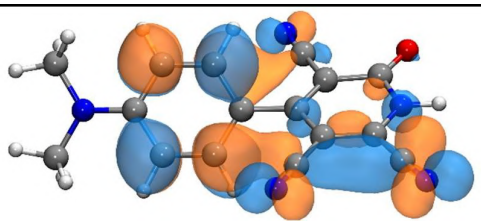
LUMO+1	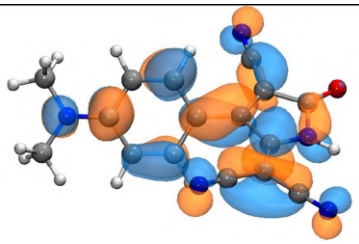	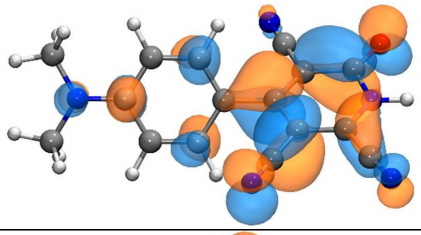
LUMO	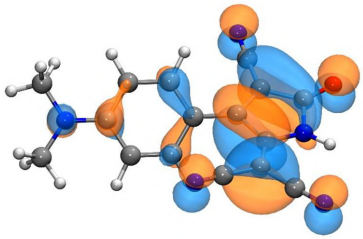	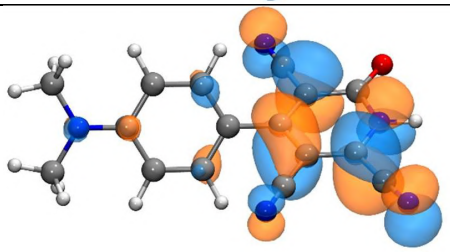
HOMO	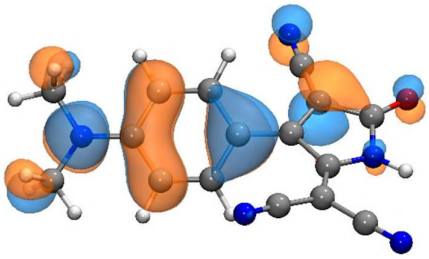	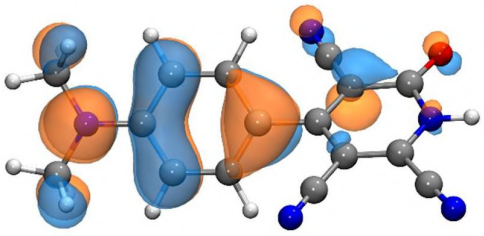
HOMO-1	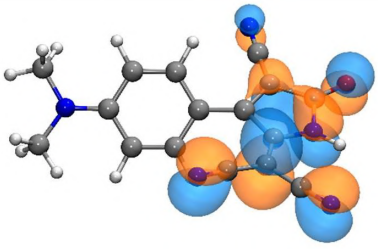	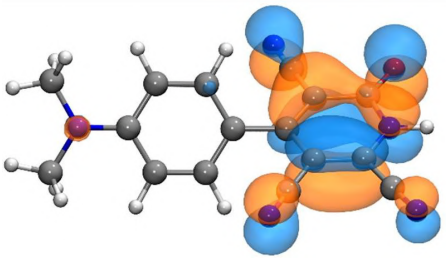
HOMO-2	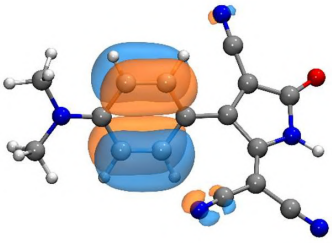	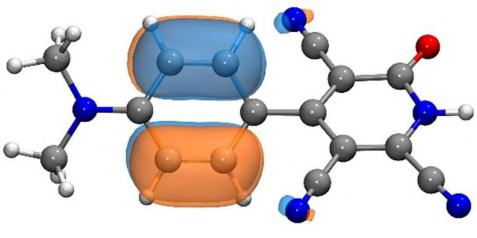

TD-DFT Calculations

The excited state calculations were carried out with time dependent DFT and accounted for 50 excited states in order to ensure that the observed spectra range is covered properly. CAM-B3LYP was chosen as a functional throughout for TD-DFT functionals. Solvent effects in CH_3CN ($\mathcal{E}$ = 36.6) were evaluated by using Conductor like Polarizable Continuum Model (CPCM) implemented in ORCA.[S9, S10]

Table S3. UV–Vis absorption spectra: excitation wavelengths, oscillator strengths (*f*) and dominant electronic transitions of **2a** in CH_3CN.

S.No	λ(nm)	*f*	Main Transitions
1	586	0.341	H → L (93.1 %)
2	309	0.209	H-3 → L (35.0%), H-2 → L (18.6%), H-1→L (31.0%)
3	286	0.390	H-3 -> L (42.0%), H-1 → L (29.2%)
4	257	0.537	H → L+1 (72.8%)
5	191	0.152	H-2 → L+1 (27.4%), H-1 → L+1 (34.2%)
6	189	0.122	H-1 → L+1 (26.0%), H → L (24.4%)

Table S4. UV–Vis absorption spectra: excitation wavelengths, oscillator strengths (*f*) and dominant electronic transitions of **3a** in CH_3CN.

S.No	λ(nm)	*f*	Main Transitions
1	517	0.184	H → L (95.2%)
2	325	0.118	H → L+1 (74.7%)
3	302	0.514	H-1 → L+1 (74.4%)
4	223	0.418	H-1→L+1 (28.8%), H-1→L+4 (25.9%), H-3→L (18.8%)
5	225	0.113	H-2 → L+1(50.3%), H-3 → L(16.7%)
6	204	0.340	H-5 → L (64.0%)
7	189	0.205	H-9 → L(31.5%), H-8 → L(18.4%)

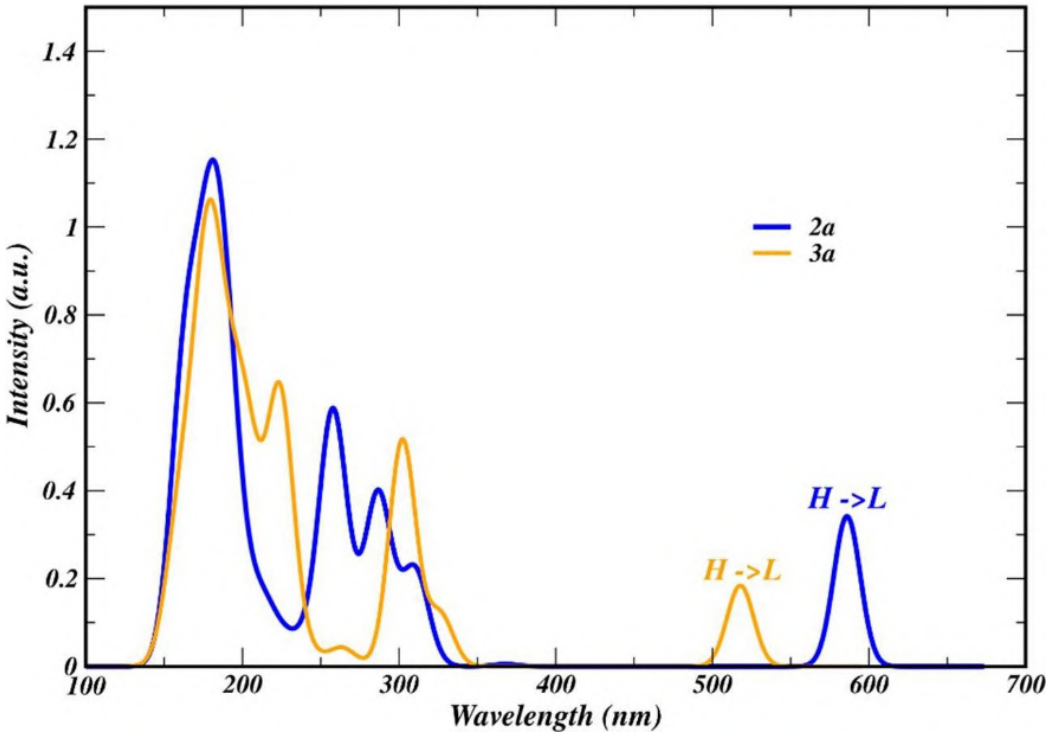

Fig. S18. UV/vis electronic spectra of **2a** and **3a** in CH_3CN obtained from TD-DFT calculations using CAM-B3LYP/def2-TZVP method.

E4 Spectral details of the synthesized compounds in the substrate scope study

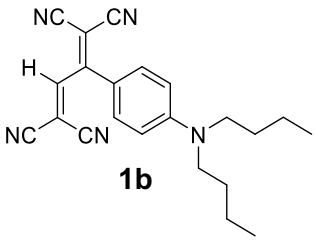

1b

^{1}H NMR (Acetone-d_6, 400 MHz, 298 K): δ = 0.97 (m, 6 H), 1.43 (m, 4 H), 1.66 (m, 4 H), 3.47 (m, 4 H), 6.87 (d, J = 9.12 Hz, 2 H), 7.33 (s, 1 H), 7.60 ppm (d, J = 9 Hz, 2H); ^{13}C NMR (100 MHz, Acetone-d_6): δ = 14.3, 20.9, 28.4, 51.5, 79.7, 109.3, 112.3, 116.0, 119.2, 127.6, 133.6, 142.4, 152.9, 167.8 ppm; HRMS (ESI): *m/z* (%) calcd. for $C_{22}H_{23}N_5^+$, $[M+H]^+$ 358.1953; found: 358.2272.

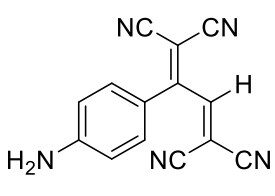

1c

1C[S11]: ^{1}H NMR (Acetone-d_6, 400 MHz, 298 K): δ = 5.62 (s, 2 H), 6.89 (d, J = 9.16 Hz, 2 H), 6.95 (s, 1H), 8.38 ppm (d, J = 11.88 Hz, 2 H); ^{13}C NMR (100 MHz, Acetone-d_6): δ = 64.9, 105.1, 114.2, 115.0, 119.3, 127.8, 133.2, 133.8, 158.8, 161.6 ppm; HRMS (ESI): *m/z* (%) calcd. for $C_{14}H_7N_5^+$, $[M+H]^+$ 246.0701; found: 246.0780.

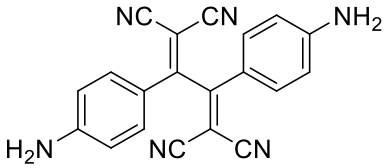

1f

1f: ^{1}H NMR ($CDCl_3$, 400 MHz, 298 K): δ = 4.59 (s, 4 H), 6.69 (d, J = 9.12 Hz, 4 H), 7.60 ppm (d, J = 9 Hz, 4 H); ^{13}C NMR (100 MHz, $CDCl_3$): δ = 110.5, 114.9, 128.6, 128.8, 132.2, 132.3, 133.0, 166.2 ppm; HRMS (ESI): *m/z* (%) calcd. for $C_{20}H_{12}N_6^+$, $[M+Na]^+$ 359.1016; found: 359.1029.

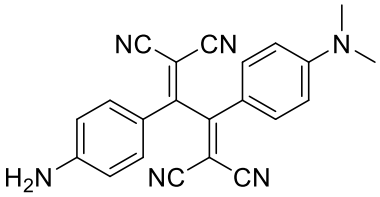

1g

1g[S12] : ^{1}H NMR ($CDCl_3$, 400 MHz, 298 K): δ = 3.14 (s, 6 H), 4.73 (s, 2 H), 6.64 (d, J = 9.1 Hz, 2 H), 6.69 (d, J = 9.24 Hz, 2 H), 7.69 (d, J = 9.24 Hz, 2 H), 7.77 ppm (d, J = 9.24 Hz, 2 H); ^{13}C NMR (100 MHz, $CDCl_3$): δ = 40.3, 60.6, 63.8, 112.2, 113.1, 113.8, 114.2, 114.8, 118.7, 120.9, 153.3, 154.4, 165.1 166.8 ppm; HRMS (ESI): *m/z* (%) calcd. for $C_{22}H_{16}N_6^+$, $[M+Na]^+$ 387.1334; found: 387.1343.

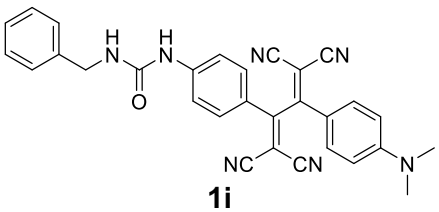

1i

1i[S13] : ^{1}H NMR (Acetone-d_6, 400 MHz, 298 K): δ = 3.18 (s, 6 H), 4.41 (d, J = 5.9 Hz, 2 H), 6.53 (t, J = 5.8 Hz, 1 H), 6.84 (d, J = 9.4 Hz, 2 H), 7.36–7.19 (m, 5 H), 7.74 (d, J = 9.04 Hz, 2 H), 7.9 (m, 4 H); 8.77 ppm (s, 1 H); ^{13}C NMR (100 MHz, acetone-d_6, 298 K): δ = 40.2, 44.2, 74.9, 83.1, 112.9, 113.7, 114.2, 114.9, 115.6, 118.2, 118.8, 127.8, 128.2, 129.2, 132.4, 133.4, 140.8, 147.9, 155.2, 155.6, 164.6, 168.0 ppm; HRMS (ESI): *m/z* (%) calcd for $C_{30}H_{23}N_7O^+$: $[M+K]^+$ 536.1601; found: 536.1615.

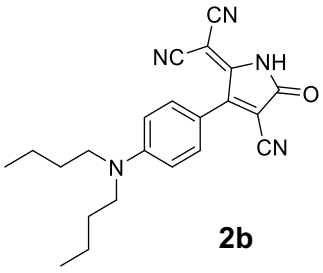

2b

^{1}H NMR ($CDCl_3$, 400 MHz, 298 K): δ = 1.0 (m, 6 H), 1.21 (m, 4 H), 1.57 (m, 4 H), 3.45 (m, 4 H), 6.76 (d, J = 9.6 Hz, 2 H), 8.12 (s, 1 H), 8.56 ppm (d, J = 9.6 Hz, 2 H); ^{13}C NMR (100 MHz, $CDCl_3$): δ = 13.9, 20.4, 25.5, 29.9, 51.6, 110.6, 112.7, 113.3, 113.70, 113.73, 116.9, 134.2, 153.8, 166.5, 169.8 ppm; HRMS (ESI): *m/z* (%)

calcd. for $C_{22}H_{23}N_5O^+$, $[M+K]^+$ 412.1534; found: 412.1550.

E4.1 NMR (^1H and ^{13}C) spectra

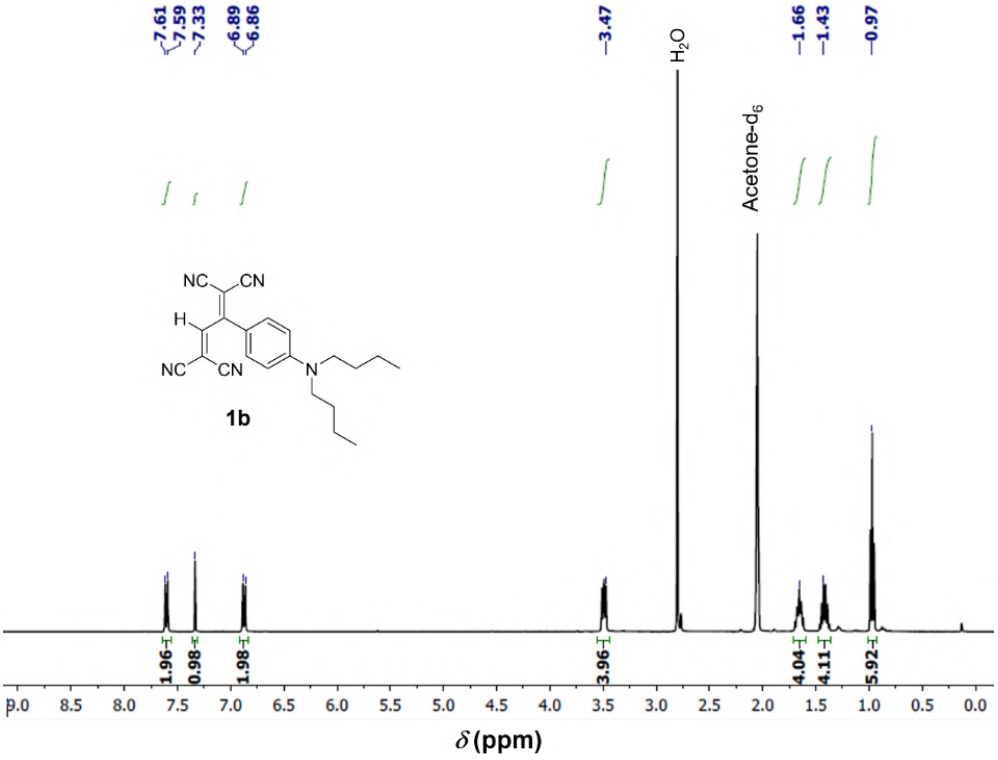

Fig. S19. 400 MHz ^1H NMR spectrum of **1b** recorded at 298 K in acetone-d_6.

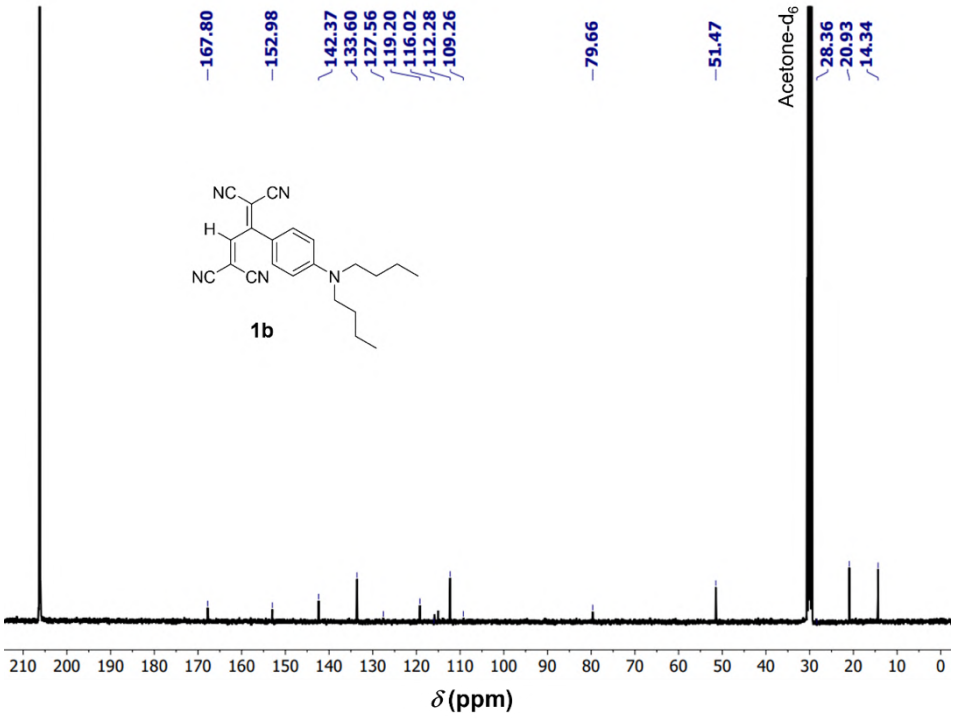

Fig. S20. 100 MHz ^{13}C NMR spectrum of **1b** recorded at 298 K in acetone-d_6.

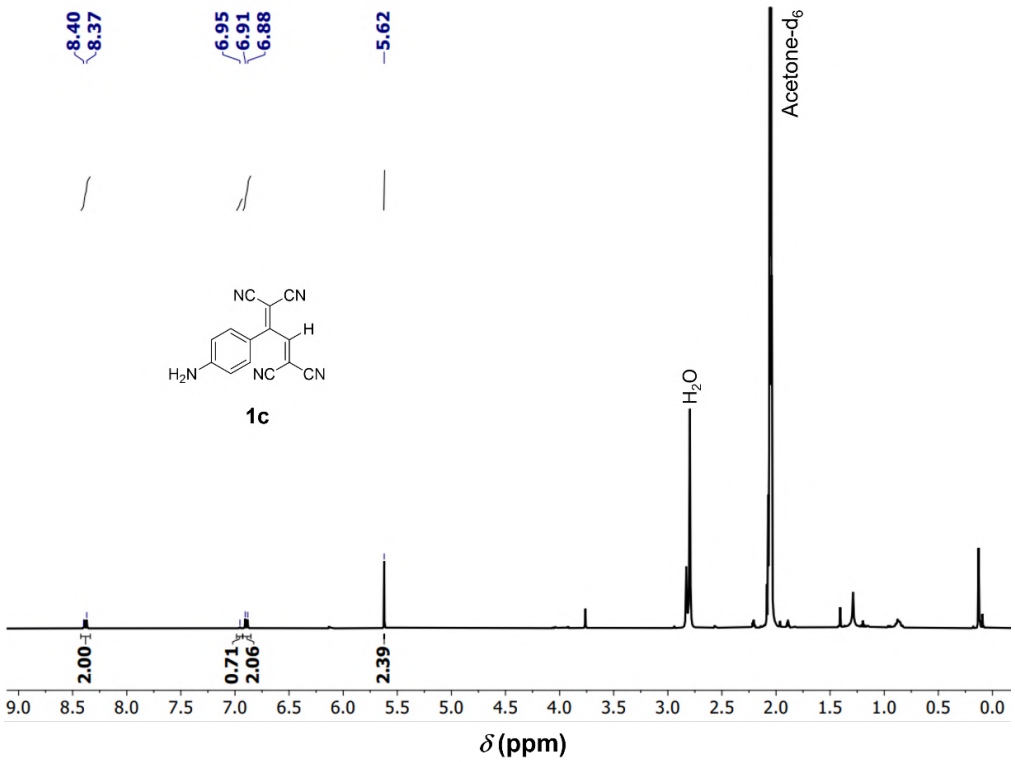

Fig. S21. 400 MHz ^{1}H NMR spectrum of **1c** recorded at 298 K in acetone-d_6.

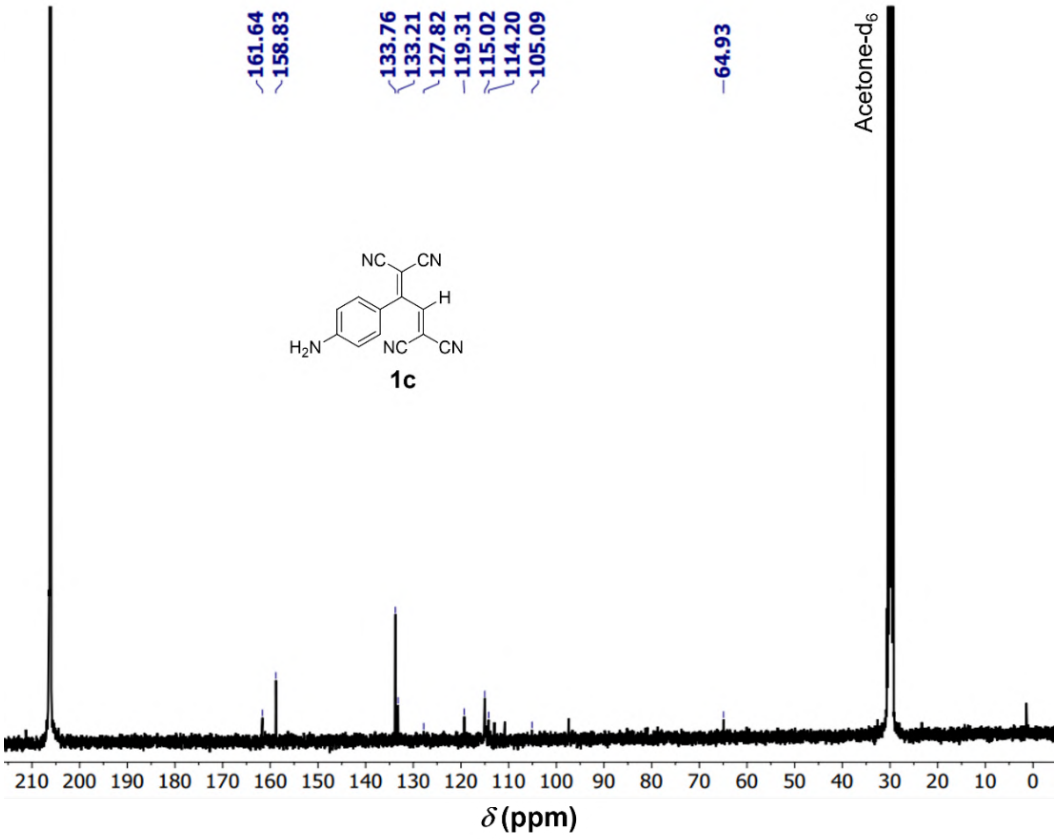

Fig. S22. 100 MHz ^{13}C NMR spectrum of **1c** recorded at 298 K in acetone-d_6.

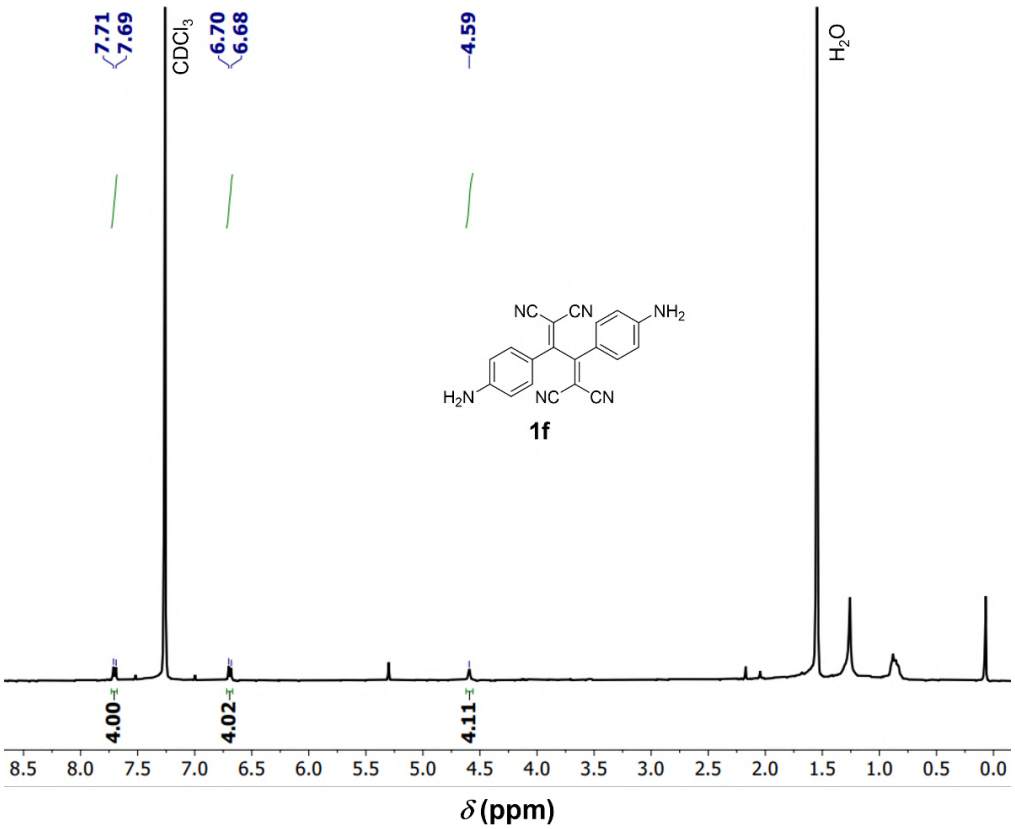

Fig. S23. 400 MHz ^{1}H NMR spectrum of **1f** recorded at 298 K in $CDCl_3$.

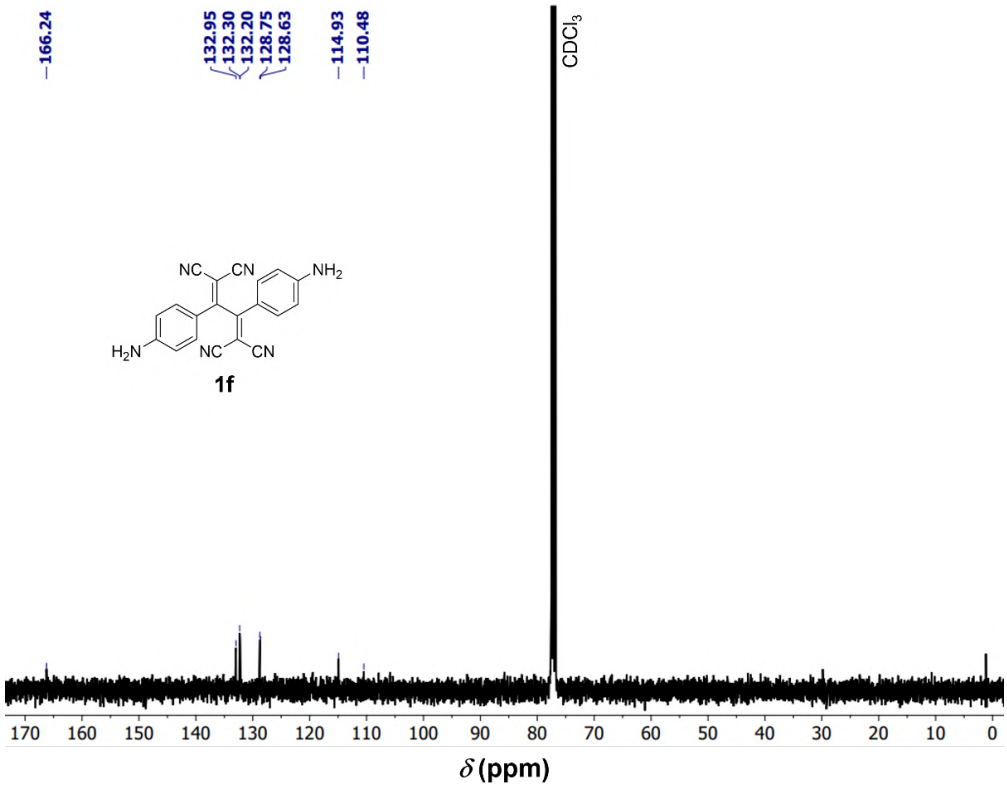

Fig. S24. 100 MHz ^{13}C NMR spectrum of **1f** recorded at 298 K in $CDCl_3$.

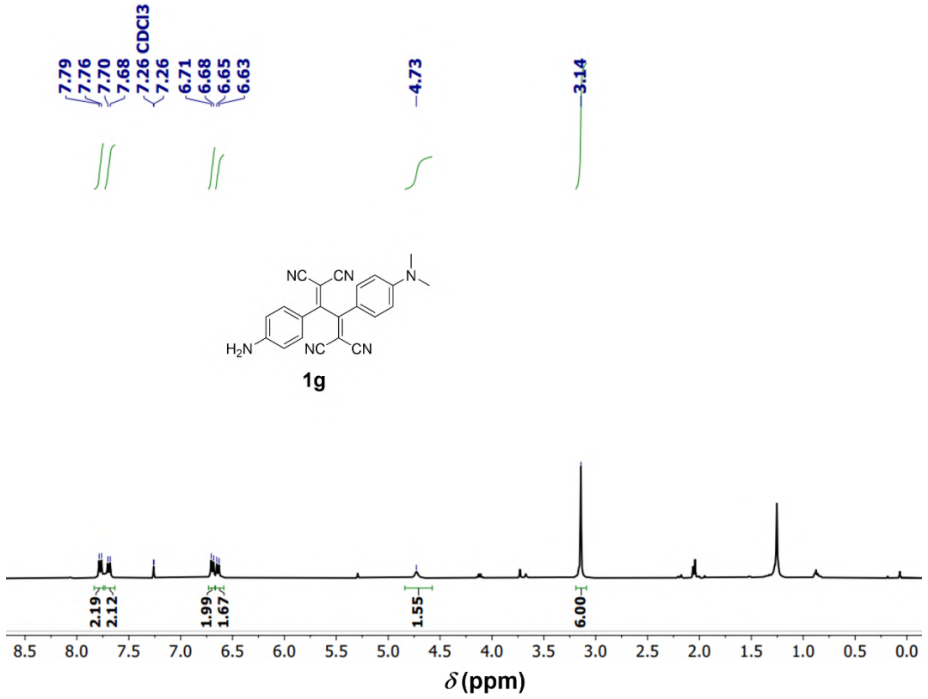

Fig. S25. 400 MHz ^{1}H NMR spectrum of **1g** recorded at 298 K in $CDCl_3$.

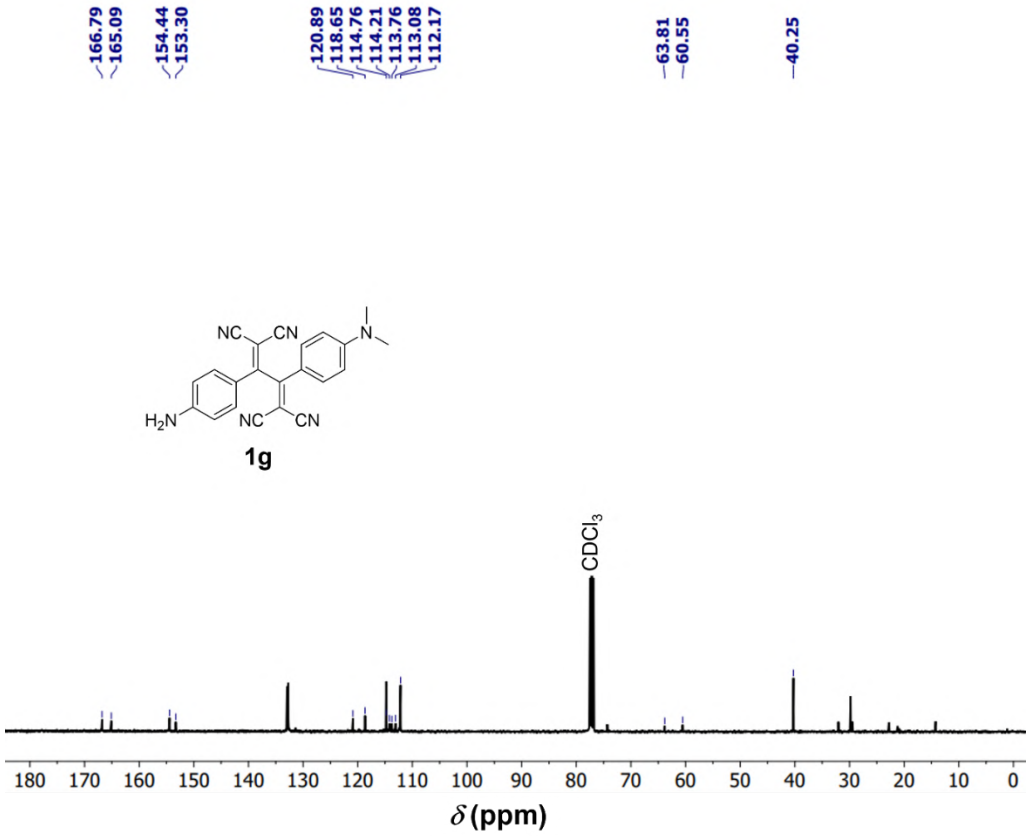

Fig. S26. 100 MHz ^{13}C NMR spectrum of **1g** recorded at 298 K in $CDCl_3$.

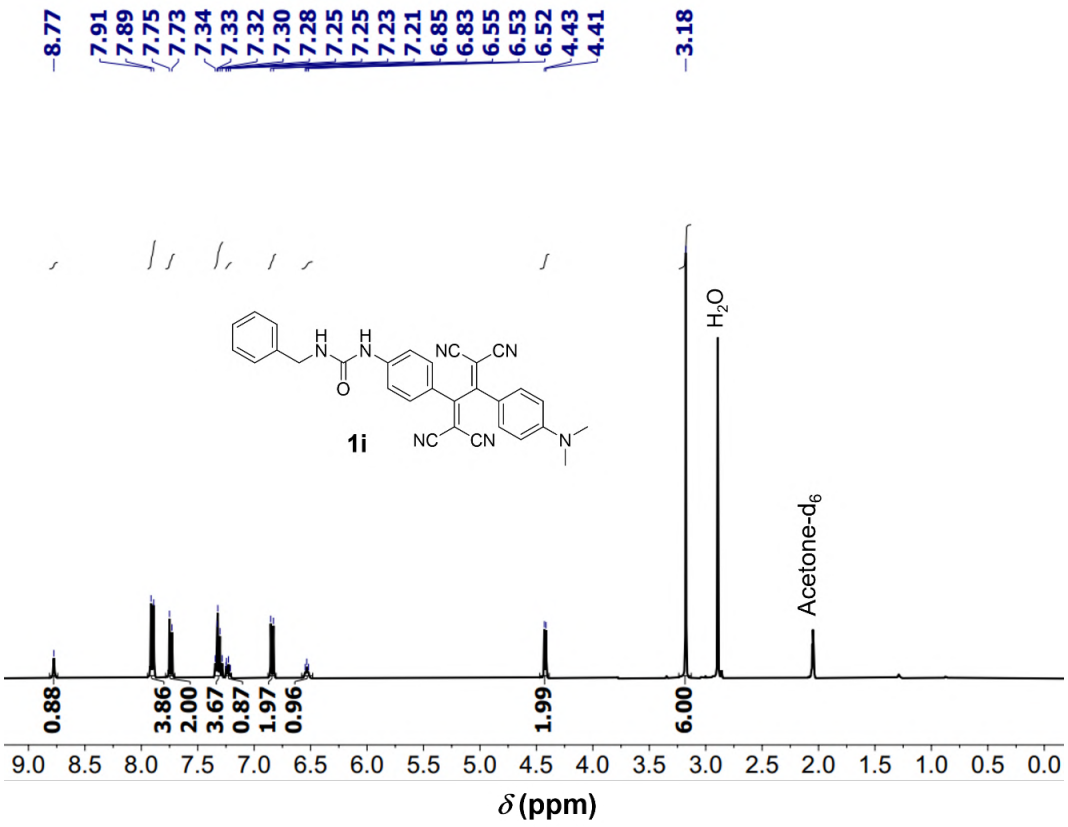

Fig. S27. 400 MHz ^{1}H NMR spectrum of **1i** recorded at 298 K in acetone-d$_6$.

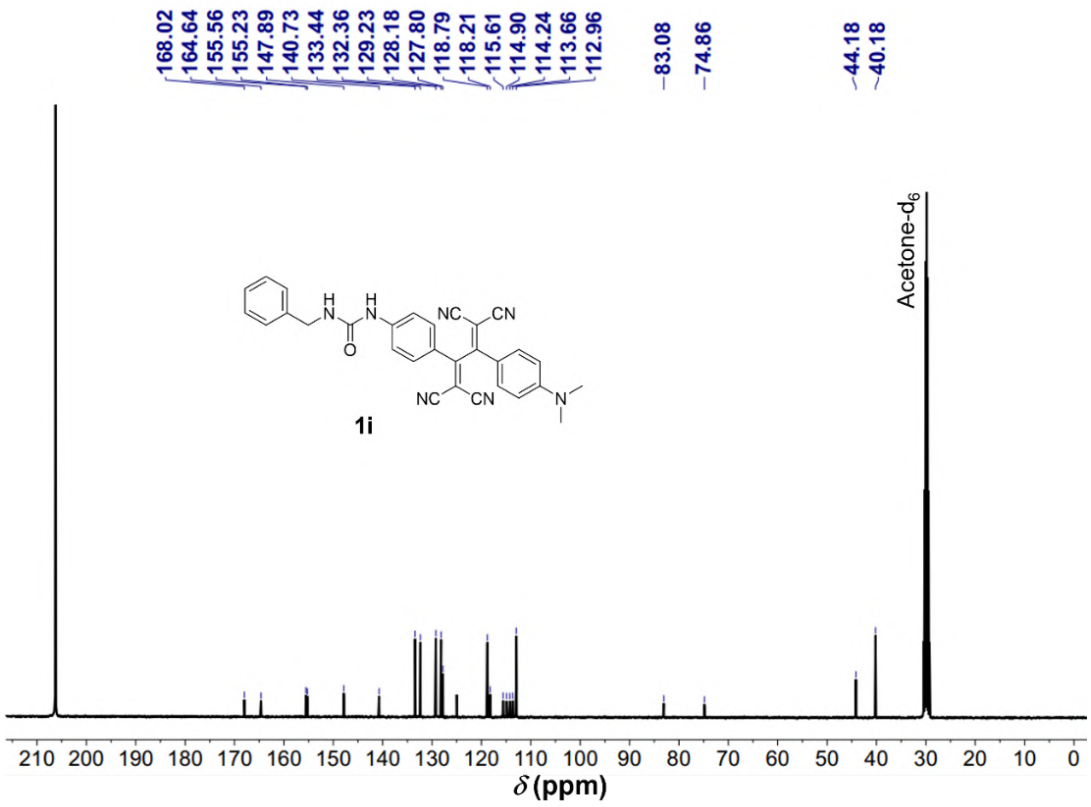

Fig. S28. 100 MHz ^{13}C NMR spectrum of **1i** recorded at 298 K in acetone-d$_6$.

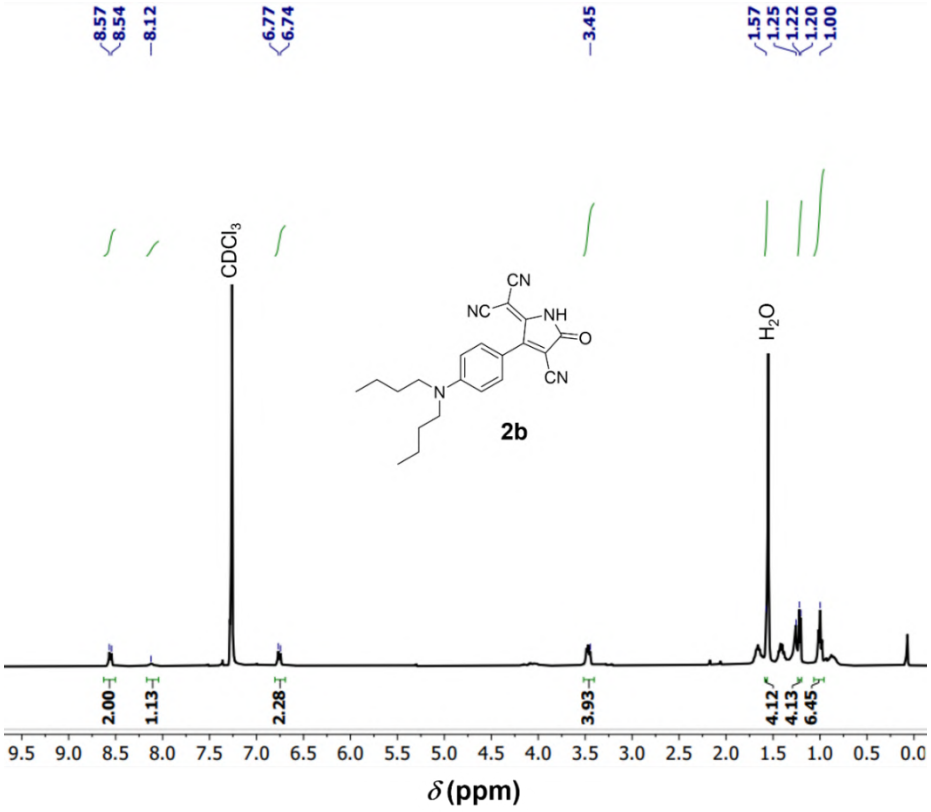

Fig. S29. 400 MHz ^{1}H NMR spectrum of **2b** recorded at 298 K in $CDCl_3$.

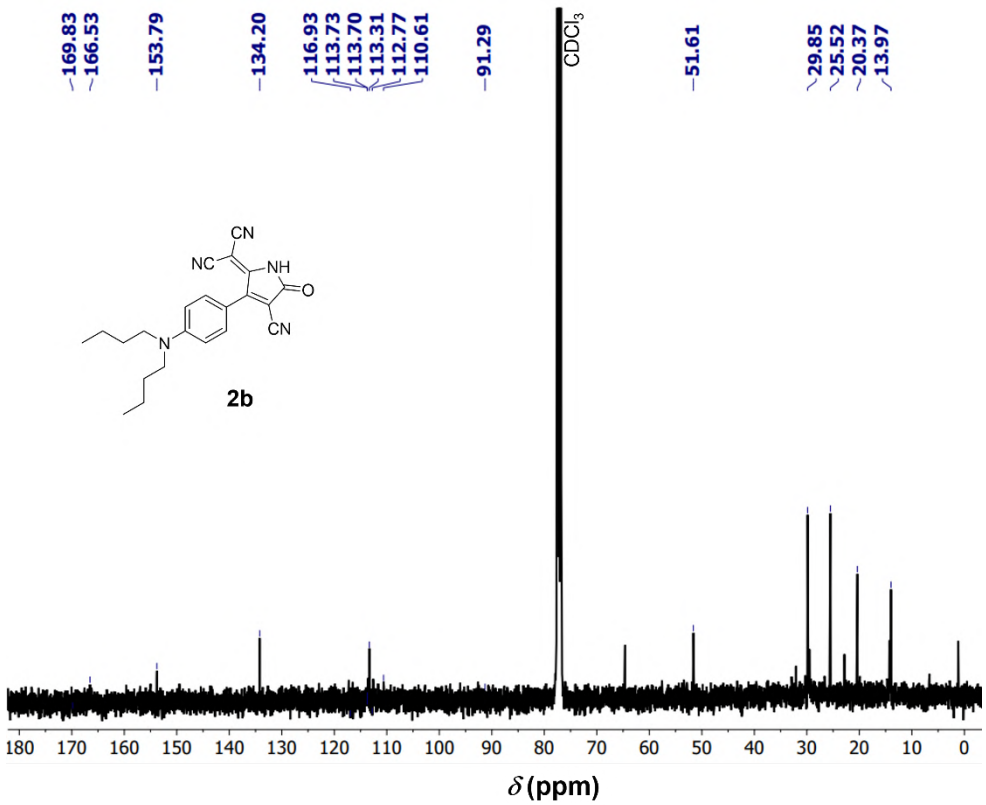

Fig. S30. 100 MHz ^{13}C NMR spectrum of **2b** recorded at 298 K in $CDCl_3$.

E4.2 ESI-MS spectra

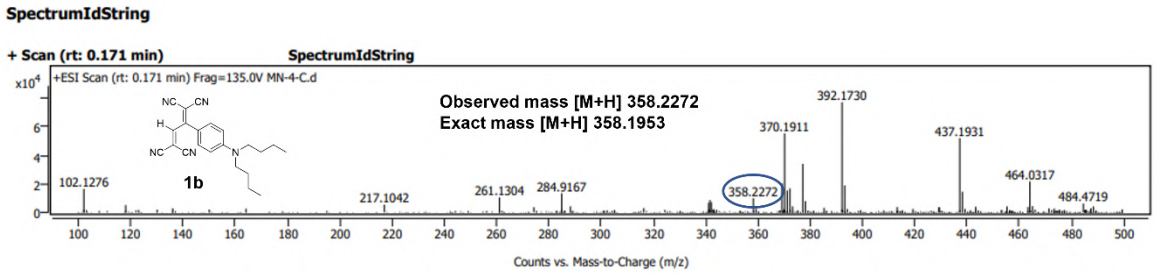

Fig. S31. HRMS spectrum of **1b**.

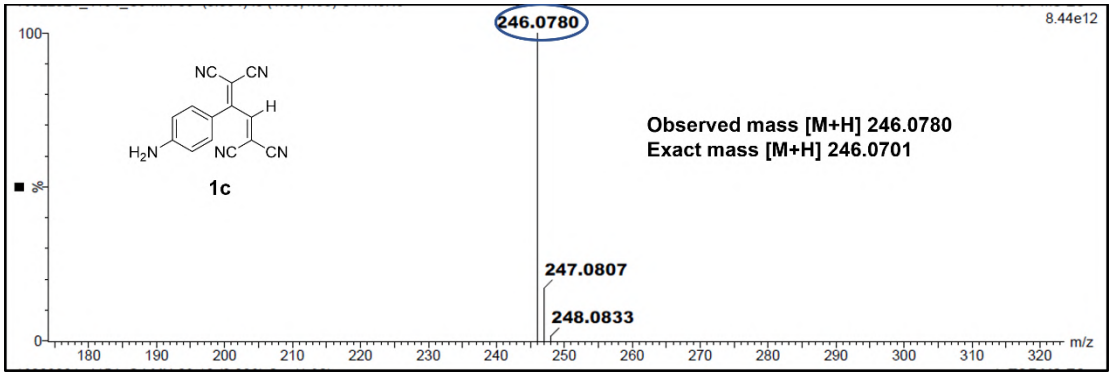

Fig. S32. HRMS spectrum of **1c**.

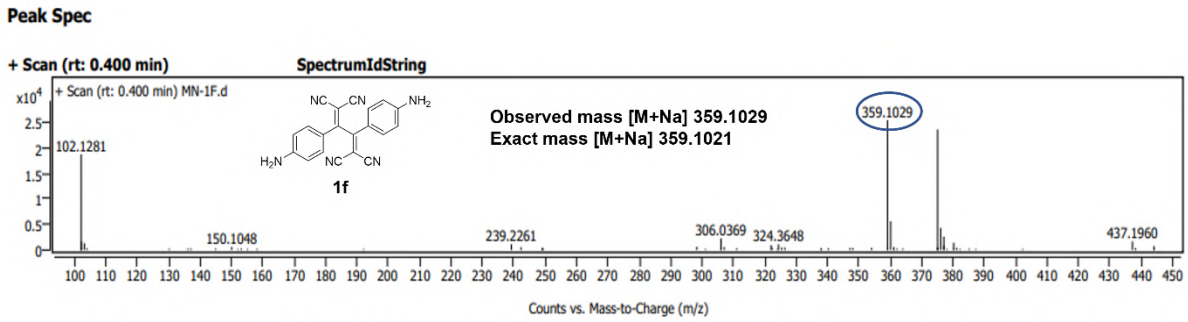

Fig. S33. HRMS spectrum of **1f**.

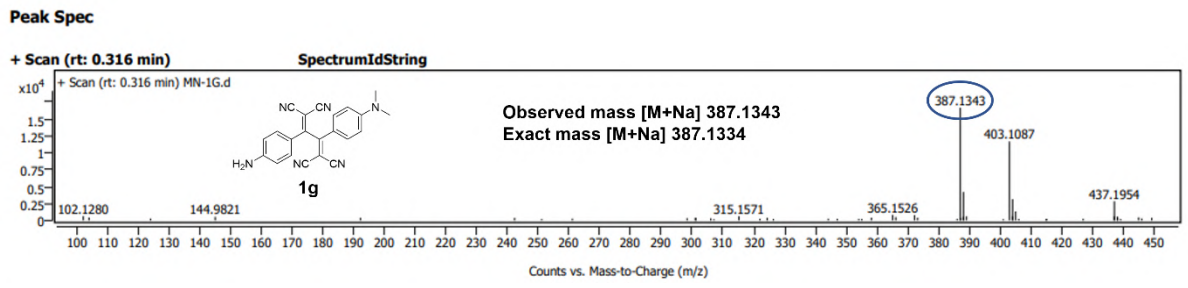

Fig. S34. HRMS spectrum of **1g**.

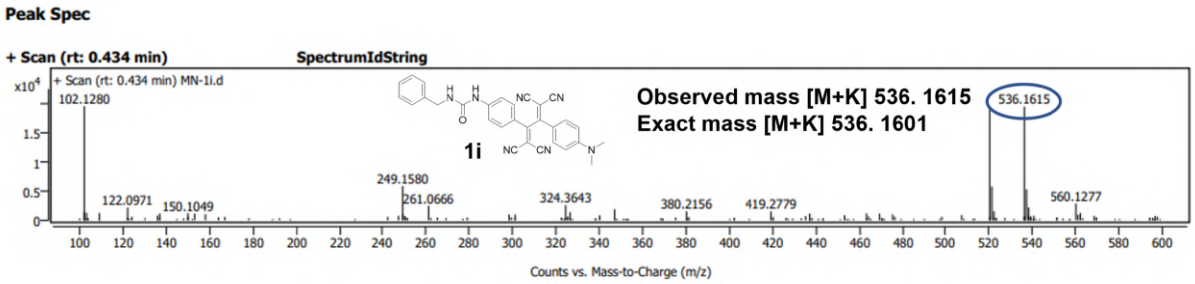

Fig. S35. HRMS spectrum of **1i**.

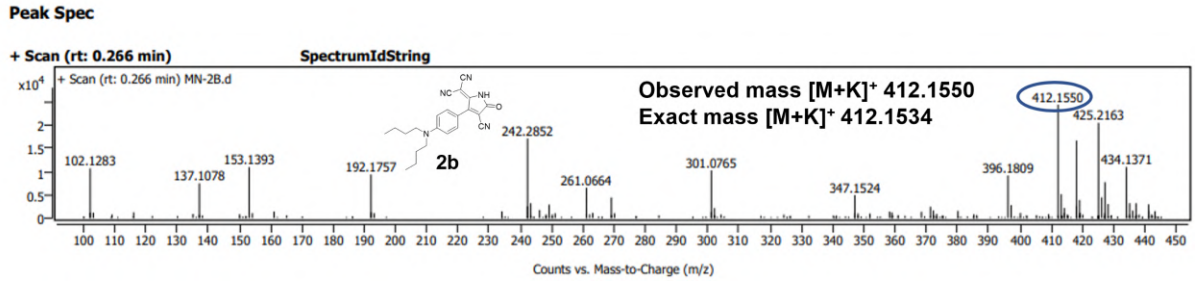

Fig. S36. HRMS spectrum of **2b**.

F References

S1. T. Michinobu, J. C. May, J. H. Lim, C. Boudon, J. -P. Gisselbrecht, P. Seiler, M. Gross, I. Biaggio, F. Diederich, *Chem. Commun.* 2005, 737–739.

S2. O. V. Dolomanov, L. J. Bourhis, R. J. Gildea, J. A. K. Howard, H. Puschmann, *J. Appl. Cryst.* 2009, **42**, 339–341.

S3. M. C. Burla, R. Caliandro, M. Camalli, B. Carrozzini, G. L. Cascarano, L. De Caro, C. Giacovazzo, G. Polidori, D. Siliqi, R. Spagna, *J. Appl. Cryst.* 2007, **40**, 609–613.

S4. G. M. Sheldrick, *Acta Cryst. C*, 2015, **71**, 3–8.

S5. a) C. Dehu, F. Meyers, J. L. Brédas, *J. Am. Chem. Soc.*, **1993**, *115*, 6198–6206; b) J. Beckmann, D. Dakternieks, A. Duthie, C. Mitchell, M. Schürmann, *Aust. J. Chem.*, 2005, **58**, 119–127.

S6. T. Michinobu, F. Diederich, *Angew. Chem. Int. Ed.*, 2018, **57**, 3552−3577.

S7. a) T. Michinobu, C. Seo, K. T. Noguchi, *Polym. Chem.*, 2012, **3**, 1427-1435; b) T. Michinobu, C. Boudon, J.-P. Gisselbrecht, P. Seiler, B. Frank, N. N. P. Moonen, M. Gross, F. Diederich, *Chem. Eur. J.* 2006, **12**, 1889−1905.

S8. F. Neese, *Wiley Interdiscip. Rev.: Comput. Mol. Sci.* 2012, **2**, 73−78.

S9. D. J acquemin, V. Wathelet, E. A. Perpete, C. Adamo, *J. Chem. Theory Comput.* 2009, **5**, 2420−2435.

S10. Y. Takano, K. N. Houk, *J. Chem. Theory Comput.* 2005, **1**, 70–77.

S11. A. R. Lacy, A. Vogt, C. Bouden, J. -P. Gisselbrecht, W. B. Schweizer, F. Diederich, Eur. *J. Org. Chem.* 2013, **5**, 869–879.

S12. T. Michinobu, C. Seo, K. Noguchi, T. Mori, *Polym. Chem.* 2012, **3**, 1427–1435.

S13. V. Gowri, S. Jalwal, Dar, A. Gopal, A. Muthukrishnan, A. Bajaj, Md. E. Ali, G. Jayamurugan, *J. Photochem. Photobiol. A.* 2021, **410**, 113163.